First-principles modeling of ferroelectric capacitors via constrained displacement field calculations

Massimiliano Stengel,[1] David Vanderbilt,[2] and Nicola A. Spaldin[3]
[1]*Centre Européen de Calcul Atomique et Moléculaire (CECAM), Station 13, Bat. PPH, 1015 Lausanne, Switzerland*
[2]*Department of Physics and Astronomy, Rutgers University, Piscataway, New Jersey 08854-8019, USA*
[3]*Materials Department, University of California, Santa Barbara, California 93106-5050, USA*
(Received 17 August 2009; revised manuscript received 23 November 2009; published 28 December 2009)

First-principles modeling of ferroelectric capacitors presents several technical challenges due to the coexistence of metallic electrodes, long-range electrostatic forces, and short-range interface chemistry. Here we show how these aspects can be efficiently and accurately rationalized by using a finite-field density-functional theory formalism in which the fundamental electrical variable is the displacement field **D**. By performing calculations on model $Pt/BaTiO_3/Pt$ and $Au/BaZrO_3/Au$ capacitors we demonstrate how the interface-specific and bulk-specific properties can be identified and rigorously separated. Then, we show how the electrical properties of capacitors of arbitrary thickness and geometry (symmetric or asymmetric) can be readily reconstructed by using such information. Finally, we show how useful observables such as polarization and dielectric, piezoelectric, and electrostrictive coefficients are easily evaluated as a byproduct of the above procedure. We apply this methodology to elucidate the relationship between chemical bonding, Schottky barriers and ferroelectric polarization at simple-metal/oxide interfaces. We find that BO_2-electrode interfaces behave analogously to a layer of linear dielectric put in series with a bulklike perovskite film while a significant nonlinear effect occurs at AO-electrode interfaces.

DOI: 10.1103/PhysRevB.80.224110 PACS number(s): 71.15.−m, 77.65.−j, 77.80.−e, 73.61.−r

I. INTRODUCTION

Capacitors based on ferroelectric perovskites hold promise for substantial advances in nanoelectronics with potential applications in nonvolatile random-access memories and high-permittivity gate dielectrics.[1] Thinner devices, which are mandatory for optimal efficiency and speed, are strongly influenced by the electrical and mechanical boundary conditions imposed by the interface.[2] While there has been significant progress in the understanding of strain effects,[3] the electrostatics of metal-ferroelectric interfaces still remains a challenge and is widely recognized as a central issue in the scaling of ferroelectric devices.

Interface electrostatics is generally modeled within Landau-Ginzburg theories, by a hypothetical thin layer of standard dielectric (dead layer) interposed between an ideal electrode and the active, bulklike ferroelectric film. The dielectric dead layer is arranged in series with the film and therefore the small interfacial capacitance associated with it tends to suppress the polarization of the film via a depolarizing field.[4] It was postulated a long time ago[5] that even in the absence of an extrinsic interfacial layer, a small interfacial capacitance can originate from the finite penetration length of the electric field in a real electrode. The imperfect-screening model and the dead-layer model are mathematically equivalent and lead to the same consequences, regardless of the microscopic nature of the effect.[6]

Owing to the complex structure and chemistry of a realistic interface, however, it is difficult to infer the magnitude of this interfacial capacitance based on macroscopic considerations. Moreover, the usual assumption that the capacitance (or equivalently, the effective screening length) is *constant* as a function of the ferroelectric displacement might not be justified in some cases. For example, it was shown very recently by means of first-principles calculations that chemical bonding across the junction profoundly influences the ferroelectric properties of the device.[7] This is likely to introduce nonlinearities in the electrical response of the interface that are neglected within most phenomenological approaches. In order to achieve a quantitative model of the electrode/ferroelectric interface there is therefore the clear need for a theory that complements Landau free-energy expansions with a microscopically reliable description of local chemistry and electrostatics.

A strategy for modeling the ferroelectric behavior of symmetric and asymmetric capacitors that combines Landau theory with first-principles calculations was recently proposed by Gerra *et al.*[8] Their strategy has the advantage of exploiting the power of the *ab initio* approach to gain quantitative insight into the coefficients that describe the behavior of the interface. In particular, the interface enters the free energy through two distinct quadratic terms, a depolarizing effect which provides a uniform electric field and is the main contribution, and a short-range chemical bonding effect which provides a much smaller correction. These coefficients are then input into a standard Landau free-energy expansion and used to predict the behavior of devices of macroscopic thicknesses, which are not directly tractable from first principles. This model was shown to describe the $SrRuO_3/BaTiO_3/SrRuO_3$ system quite accurately. The results were consistent with the seminal work of Junquera and Ghosez,[9] who demonstrated how the main impact of the electrodes is embodied in the depolarizing field in an otherwise bulklike $BaTiO_3$ (BTO) film.

Some authors, however, have questioned the generality of such an assumption, postulating that in some cases the electrodes can have a much more profound impact on the ferroelectric film. The authors of Ref. 10, for example, claimed that $SrRuO_3$ electrodes can destroy the polar soft mode of ferroelectric $KNbO_3$ films, producing a head-to-head domain

wall a few unit cells from the interface. Furthermore, in Ref. 11, Pt electrodes were found to induce a "ferrielectric" dipole pattern in the whole volume of a $BaTiO_3$ film. Such effects, which are nonlocal in nature, cannot be described by the simple models of Refs. 8 and 9. To account for (and clarify the nature of) these "exceptions," it would be very desirable to have a rigorous methodological framework that treats the electrical properties of a given capacitor heterostructure fully from first principles without any *a priori* assumptions.

Such a methodological framework was recently developed for the case of purely insulating perovskite superlattices. By performing the calculations at a fixed value of the electric-displacement field D, Wu *et al.*[12] were able to separate the long-range electrostatic interactions between layers from the short-ranged compositional dependence. Based on this separation, the electrical properties of a given layer were shown to depend on the chemical nature of a small number of first and second neighbors only. This allowed for a first-principles description of dielectric, ferroelectric, and piezoelectric properties of arbitrary superlattice sequences in terms of very few parameters, appropriately arranged in the form of a cluster expansion.

It is the main scope of this work to extend these ideas to the case of ferroelectric films with metallic electrodes. Such an extension is now possible as there are well-established methods for treating polarization and electric fields in metal/insulator heterostructures, and these can readily be combined with recently developed approaches for treating the electric displacement field D as the controlled electric variable.[7,12,13] Using an extensive analysis of several $Pt/BaTiO_3/Pt$ and $Au/BaZrO_3/Au$ capacitor heterostructures to illustrate the power of this approach, we show that a film-electrode interface behaves analogously to an insulator-insulator interface in a ferroelectric superlattice (assuming that there is no Schottky breakdown) in that the same "locality principle"[12] holds. This means that the film is in a bulklike state except for the two or three oxide monolayers which lie closest to the boundary. Moreover, all the complexity of interfacial chemical bonding and electrostatics can be incorporated in a single energy contribution, which we define as the interface electric equation of state. Taking advantage of the constrained-D technique, we further show how to extract in practice (from calculations of compositionally *symmetric* capacitors) such an interface equation of state and represent it in terms of a potential drop which is in general a nonlinear function of the electric displacement field. Then, we use this information, together with the bulk equation of state of the ferroelectric, to predict, with full first-principles accuracy, the electrical properties of capacitors of arbitrary thickness and geometry (symmetric or asymmetric). Finally, we show how useful observables such as polarization and dielectric, piezoelectric, and electrostrictive coefficients are easily evaluated as a byproduct of the above procedure.

Our results demonstrate the validity of D as a fundamental electrical variable to study ferroelectric capacitors within an imperfect screening regime. (The appropriateness of such an approach was recently questioned although in a slightly different context, in Ref. 14.) From the practical point of view, our detailed study of $Au/BaZrO_3/Au$ capacitors also yields important insight into the similarities and dissimilarities of AO-terminated versus BO_2-terminated perovskite films in contact with simple-metal electrodes. On the one hand, the relatively high interfacial capacitances we obtain for both interface types corroborate the ideas of Ref. 7, where weak interface bonding was found to be favorable for the overall dielectric (or ferroelectric) response of the device. On the other hand, at the BaO-Au interface we find significant nonlinear effects, which do not fit into a "constant interfacial capacitance" model. We correlate these effects with the formation and breaking of the interfacial Au-O bonds upon polarization reversal. (This same mechanism was already found to strongly influence the ferroelectric instability in Ref. 7.)

The manuscript is structured as follows. In Sec. II we review the methodological background and present the developments which are specific to this work. In Sec. III we discuss the structural and electronic properties of ferroelectric $Pt/BaTiO_3/Pt$ capacitors, which we then use to model their dielectric and piezoelectric properties as a function of thickness and applied bias. In Sec. IV we focus on the $Au/BaZrO_3/Au$ model system. First we compare the electrical properties of the Au-BaO and the Au-ZrO_2 interface structures then we show how to reconstruct the behavior of asymmetric capacitor configurations starting from the interfacial and bulk equations of state. Finally, in Secs. V and VI we discuss our results in light of the existing literature and present our conclusions.

II. METHODS

A. Polarization

1. Bulk insulators

We shall consider superlattices and capacitor structures stacked along $\hat{z}$ so that we are interested in polarizations and fields only along this direction. We start with the case of a bulk insulator, either a single bulk unit cell or a supercell representing an insulating superlattice but with a formulation chosen for convenient later generalization to the case of a capacitor structure.

We thus consider a periodic insulator described by three real-space lattice vectors $\mathbf{R}_i$, where for simplicity of notation we impose that $\mathbf{R}_3=(0,0,c)$ is perpendicular to $\mathbf{R}_{1,2}$ (the latter two lie therefore in the xy plane); the corresponding reciprocal-space vectors are $\mathbf{G}_{1,2,3}$. We choose a discrete k-point sampling of the form $\mathbf{k}=j\mathbf{b}_\parallel+\mathbf{k}_\perp$, where the vector $\mathbf{b}_\parallel=\mathbf{G}_3/N_\parallel$ spans a regular one-dimensional (1D) mesh of dimension $N_\parallel$, and $\mathbf{k}_\perp$ belongs to a set of $N_\perp$ special points in the perpendicular plane. The electronic ground state is defined by a set of one-particle Bloch orbitals, $u_{n\mathbf{k}}$; our goal now is to define the polarization along $\mathbf{G}_3$.

To that end, we first seek a localized representation of the electronic wave functions along the direction $\mathbf{G}_3$ for each given $\mathbf{k}_\perp$. We do this by constructing a set of maximally localized "hermaphrodite" orbitals $w_{n\mathbf{k}_\perp}(\mathbf{r})$ that are Wannier-type along z while remaining Bloch-type in the xy plane[15,16] using a parallel-transport procedure.[17] The center $z_{n\mathbf{k}_\perp}$ of $w_{n\mathbf{k}_\perp}$ is then defined as[18]

$$z_{n\mathbf{k}_\perp} = \langle w_{n\mathbf{k}_\perp} | \hat{z} | w_{n\mathbf{k}_\perp} \rangle = \int |w_{n\mathbf{k}_\perp}(\mathbf{r})|^2 z dr^3 \quad (1)$$

and the contribution of $\mathbf{k}_\perp$ to the polarization is

$$P(\mathbf{k}_\perp) = \frac{1}{\Omega}\left(-2e\sum_n z_{n\mathbf{k}_\perp} + \sum_\alpha Q_\alpha z_\alpha\right), \quad (2)$$

where z_α and Q_α are the ionic coordinate and bare pseudopotential charge, respectively, of the atom α; the factor of two refers to spin-paired orbitals. The total polarization P is then obtained by integrating $\mathbf{k}_\perp$ over its two-dimensional (2D) Brillouin zone while making sure that the branch choice of $P(\mathbf{k}_\perp)$ is continuous in $\mathbf{k}_\perp$. This integration is performed by using the special-point technique with a discrete set of $\mathbf{k}_\perp$ and associated weights $\bar{w}_{\mathbf{k}_\perp}$

$$P = \sum_{N_\perp} \bar{w}_{\mathbf{k}_\perp} P(\mathbf{k}_\perp).$$

Note that the integration along the polarization direction is implicit in the construction of the Wannier functions; therefore, only a 2D integration of $P(\mathbf{k}_\perp)$ is needed. Note also that we included the ionic contribution in the definition of $P(\mathbf{k}_\perp)$. This might look surprising at first sight as the ionic charges and positions are independent of $\mathbf{k}_\perp$. Indeed, it would have been perfectly equivalent if we integrated the electronic contribution first and only in the end added the ionic part. However, the electronic-only part is not a well-defined physical quantity as it is not charge neutral and therefore origin dependent. For this reason, we preferred the present formulation, which yields identical results while providing a function $P(\mathbf{k}_\perp)$ that is origin independent.

Our Wannier-based definition of P, Eq. (2), lends itself naturally to a local decomposition in terms of the dipolar contribution of individual oxide layers as proposed in Refs. 12 and 19. In particular, given that in typical perovskite insulators the centers $z_{n\mathbf{k}_\perp}$ cluster themselves around the oxide layers they formally "belong" to, one can define the layer polarization (LP) of the jth layer as

$$p_j(\mathbf{k}_\perp) = \frac{e}{S}\left(-2\sum_{n\in j} z_{n\mathbf{k}_\perp} + \sum_{\alpha\in j} Q_\alpha Z_\alpha\right). \quad (3)$$

In the above equation the sums are restricted to atoms α and Wannier centers i that are "in" the layer j, and S is the cell surface area; again, the overall p_j is calculated by performing a 2D Brillouin-zone average. p_j is well defined as long as (i) the oxide layers are charge-neutral and (ii) the assignment of a specific atom or wave function to a given layer is clear cut and unambiguous. Both conditions are satisfied in typical II-IV perovskite ferroelectrics such as $PbTiO_3$ and $BaTiO_3$.

2. Capacitor superlattices

Ideally one would like to study a capacitor in the form of a number of layers of insulator sandwiched between semi-infinite metallic contacts. However, we adopt here the standard approach of constructing supercells consisting of alternating insulating and metallic regions stacked along z, just as is normally done when studying ferroelectric superlattices. We adopt the same notations and conventions as in Sec. III A with c being the superlattice repeat distance along z. We set $N_\parallel = 1$ (and henceforth write $\mathbf{k}_\perp = \mathbf{k}$); this is by no means a limitation since we are only interested in capacitors that are thick enough so that tunneling is insignificant, in which case the one-particle bands will have negligible dispersion along the z direction. We further require a rectifying (rather than Ohmic) contact at the oxide/electrode interface. This means that both the valence-band maximum (VBM) and conduction-band minimum (CBM) of the film are located far enough in energy from the Fermi level that they are not appreciably populated/depleted by the tails of the smearing function (e.g., Fermi-Dirac, Gaussian, etc.).

Because the capacitor superlattice is metallic, one might wonder whether it is possible to define a polarization P. However, the superlattice is only metallic in the x and y directions, whereas we are interested only in computing P along z, and only in applying fields along z. The methodology for computing P in such cases was developed in Ref. 20. The electronic states are classified into three energy windows: (i) the completely empty states (upper window) are discarded from the computation since they do not contribute to P or to other ground-state properties. (ii) The partially occupied states (middle window) lying in the range $\mathcal{W} = [E_F - \delta, E_f + \delta]$ around the Fermi level E_f are considered as *conduction* states. Since these states fall in the energy gap of the dielectric film, they are confined to the metallic slab and the dipole moment of their overall charge distribution is thus well defined. To make sure that this conduction charge distribution decays fast enough in the insulating film, it is useful to define its planar average

$$\rho_{\text{cond}}(z) = \frac{1}{S}\sum_{\epsilon_{n\mathbf{k}}\in\mathcal{W}} w_{\mathbf{k}} f_{n\mathbf{k}} \int dxdy |\psi_{n\mathbf{k}}(\mathbf{r})|^2, \quad (4)$$

where $\epsilon_{n\mathbf{k}}$ and $f_{n\mathbf{k}}$ are the eigenvalue and occupancy of the state, $w_{\mathbf{k}}$ is the k-point weight, and S is the cell cross-sectional area. (iii) The lower states, which are all fully occupied are transformed to yield a set of hybrid Wannier functions $w_{\mathbf{k}n}$ that are maximally localized along z while remaining extended (and labeled by $\mathbf{k} = \mathbf{k}_\perp$) in the x and y directions. The contribution of each Wannier function to P is then defined through the center of the corresponding charge distribution $\rho_{\mathbf{k}n}(x) = |w_{\mathbf{k}n}(x)|^2$.

The center of charge of $\rho_{\text{cond}}(z)$ (middle window) is computed by integrating against a linear sawtooth function whose discontinuity is placed in the middle of the insulating region. Similarly, the center of each Wannier charge (lower window) is computed from its $\rho_{\mathbf{k}n}$ using a sawtooth function whose discontinuity is chosen far away from its center. For the systems considered in this work, the $\rho_{\mathbf{k}n}$ are typically very well localized and the main source of error comes from the slower decay length of ρ_c in the insulator. This means that in very thin capacitors (few oxide layers) the polarization becomes ill defined; rather than a defect of the algorithm, this is a signature that the system becomes metallic and the polarization cannot be defined.

Note that there is an inherent arbitrariness in the separation of the total charge density into lower and middle win-

dows (i.e., in the choice of the parameter δ above). This arbitrariness indeed affects both ρ_{cond} and those $\rho_{\mathbf{k}n}$ which lie closest to the electrode; the total value of P, however, is not affected by this choice and is therefore well defined. Far enough from the electrode, the $\rho_{\mathbf{k}n}$ themselves are unaffected by this choice and can therefore be used to construct meaningful layer polarizations analogously to the case of an insulating superlattice. This point will be demonstrated in practice in the applications sections.

We are generally concerned with capacitor structures in which a finite bias is applied across the capacitor. In our approach, this is treated by applying a finite macroscopic electric field $\mathcal{E}$ along the z direction of the superlattice and identifying $\mathcal{E}c$ as the bias applied between successive metallic segments. The formulation above applies equally well to this case, where it is understood that the electric field couples to ρ_{cond} (middle window) and to all the Wannier charges (lower window). Note that the presence of a finite macroscopic field implies that there are effectively an infinite number of regularly spaced Fermi levels, one for each repeated image of the metallic slab along the field direction. The "transition" between two adjacent Fermi levels takes place deep in the insulating slab, where the system is locally insulating and a shift in E_{f} within the gap does not produce any physical consequence.

B. Constrained-D method

1. General theory

We summarize here the details of the constrained displacement-field method that are most relevant for this work (see Ref. 13 for the full derivation). For consistency with the previous sections, we restrict our analysis to the case of a monoclinic system with the polarization axis, z, parallel to the heterostructure stacking direction and perpendicular to the xy plane; we shall further assume that $\mathbf{R}_{1,2}$ are fixed and only c (together with the ionic and electronic coordinates, $\{v\}$) is allowed to vary. Within these assumptions, the constrained-$\mathbf{D}$ method[13] reduces to a simpler formulation, where only the z components of the macroscopic fields $\mathbf{D}$, $\mathbf{P}$, and $\boldsymbol{\mathcal{E}}$ are explicitly treated. Thus, we define the internal energy functional

$$U(D,\{v\},c) = E_{KS}(\{v\},c) + \frac{Sc}{8\pi}[D - 4\pi P(\{v\},c)]^2, \quad (5)$$

which depends directly on the external parameter D, and indirectly on the internal ($\{v\}$) and strain (c) variables through the Kohn-Sham total energy E_{KS} and the macroscopic polarization P; $S=|\mathbf{R}_1 \times \mathbf{R}_2|$ is the constant cell cross section. We then proceed to minimize the functional with respect to v and c at fixed D

$$U(D) = \min_{\{v\},c} U(D,\{v\},c), \quad (6)$$

which yields the equilibrium state of the system as a function of the electric displacement D.

D can also be expressed in terms of the reduced variable $d=SD/4\pi$, which has the dimension of a charge and can be interpreted as $d=-Q_{\text{free}}$, where Q_{free} is the free charge per surface unit cell stored at a hypothetical electrode located at $z=+\infty$.[21] Since the surface areas of the parallel plate capacitors considered in this study are not allowed to vary, constraining D or d is completely equivalent. However, for reasons of convenience, we shall adopt d as our electrical variable in the remainder of this work.

This method is equally valid for bulk insulators, insulating superlattices, and capacitor superlattices, once the polarization is defined as explained in Sec. II A. For the capacitor case, our adoption of the definitions of Sec. II A 2 implies that the metallic electrode layer is treated as an infinitely polarizable dielectric and the free charges on its surfaces are reinterpreted as polarization charges coming from the metal. While such a choice may seem unnatural from the point of view of textbook electrostatics, it is in fact the most natural one in the context of first-principles electronic-structure calculations, where it is not easy to draw a distinction between free and bound charges. For example, the metal-insulator interface is typically rather diffuse with the conduction states of the metal mixing strongly with the states of the insulator across several interatomic spacings so that a spatial distinction is not meaningful and we have seen in Sec. II A 2 that a distinction based on energy windows is also arbitrary to some degree.

The reduced electric field $\bar{\varepsilon}=\mathcal{E}c$, which is minus the potential step across the supercell, $\bar{\varepsilon}=-V$, is related to the internal energy by

$$\bar{\varepsilon}(d) = \frac{dU(d)}{dd}. \quad (7)$$

This corresponds to the fundamental relationship

$$U(D_2) - U(D_1) = \frac{\Omega}{4\pi}\int_{D_1}^{D_2} \mathcal{E}(D)dD \quad (8)$$

of classical electrostatics but expressed in differential form using the reduced variables appropriate to the variable-cell case. The connection to classical electrostatics can be made even more apparent by recalling the relationship between the reduced variables and free charges and potentials

$$U(D_2) - U(D_1) = \int_{d_1}^{d_2} \bar{\varepsilon}(d)dd = \int_{Q_1}^{Q_2} V(Q)dQ. \quad (9)$$

Having established the functional relationships between the active degrees of freedom (both electrical and structural), it is relatively easy now to extract from a calculation all functional properties of a material or device that involve a coupling between them. For example, the *proper* piezoelectric strain constant can be readily obtained as

$$d_{33} = \frac{dc}{d\bar{\varepsilon}} = \frac{dc}{dd}\left(\frac{d\bar{\varepsilon}}{dd}\right)^{-1}. \quad (10)$$

Note that in the above equation $d\bar{\varepsilon}/dd$ has the dimension of an inverse capacitance and is related to the free-stress dielectric constant of the crystal; with the notation of Ref. 22 we have

$$\epsilon_{33}^{(\sigma)} = \frac{4\pi c}{S}\left(\frac{d\bar{\varepsilon}}{dd}\right)^{-1}. \quad (11)$$

2. Practical procedure

We typically span the range of relevant polarization states by repeating the structural and electronic relaxations for a number (five to ten) of equally spaced d values, $d=d_1,d_2,\ldots,d_n$. For each d_i, we tabulate the energy U_i, (cell-averaged) electric field $\mathcal{E}_i$ and equilibrium out-of-plane lattice constant c_i; we use the latter two to compute the reduced field $\bar{\varepsilon}_i=\mathcal{E}_i c_i$.

In order to obtain $\bar{\varepsilon}_i$ with sufficient accuracy it is important to perform well-converged structural relaxations by imposing sufficiently stringent thresholds on residual forces and stresses. A useful indicator of the overall numerical quality of the calculations is the fundamental relationship Eq. (7), which, in principle, should be exactly satisfied. To check the validity of Eq. (7) we first perform a polynomial fit to the calculated $(\bar{\varepsilon}_i,d_i)$ points. This yields a continuous function, $\bar{\varepsilon}(d)$ that we integrate analytically to obtain $U(d)$ modulo a constant; we choose this constant as the one that best matches the first-principles internal energies (U_i,d_i). Any residual discrepancy between U_i and $U(d_i)$ points to a numerical issue that must be addressed before proceeding further in the analysis. Usually the most important source of error concerns the relaxation of the cell volume and shape; we shall discuss this issue further in Sec. II E. For convenience, we also perform a polynomial fit to the (c_i,d_i) points, which yields a continuous curve $c(d)$ that is relevant for the piezoelectric response of the crystal as stated in Sec. IV B.

C. Locality principle and spatial decomposition

According to classical electrostatics, in the absence of free charge the normal component of the electric displacement field is preserved at a planar interface between two insulators

$$(\mathbf{D}_2-\mathbf{D}_1)\cdot\hat{\mathbf{n}}=0. \quad (12)$$

This means that for an insulating superlattice in electrostatic equilibrium, D is the same in all participating layers, unlike the electric field $\mathcal{E}$ and the polarization P, whose local values generally vary from layer to layer (see Fig. 1). Therefore, using D (or d) as the fundamental electrical variable is extremely practical for modeling the behavior of ferroelectric capacitors because it makes it possible to decompose the equation of state of a layered structure into the sum of the individual building blocks.

For example, we can write the internal energy as

$$U(d)=\sum_i U_i(d), \quad (13)$$

where U_i refers to the internal energy of an appropriately defined subunit. For a capacitor with metallic electrodes, it is natural to decompose the internal energy as

$$U(d)=\bar{U}_{\mathrm{L}}+U_{\mathrm{L}}(d)+NU_{\mathrm{b}}(d)+U_{\mathrm{R}}(d)+\bar{U}_{\mathrm{R}}, \quad (14)$$

where N is the number of bulk cells comprising the insulating film and U_{b} is its bulk internal energy per cell, $U_{\mathrm{L}}(d)$ and $U_{\mathrm{R}}(d)$ are the left (L) and right (R) interface internal energies, and $\bar{U}_{\mathrm{L}}$ and $\bar{U}_{\mathrm{R}}$ are the internal energies of the left and right metallic electrodes. (In our capacitor supercells, $\bar{U}_{\mathrm{L}}$ and $\bar{U}_{\mathrm{R}}$ are combined into $N_{\mathrm{metal}}U_{\mathrm{metal}}$, where N_{metal} is the number of cells of bulk metal and U_{metal} is its internal energy per cell, which is independent of d as appropriate for a metal.) Taking the derivative of Eq. (14) according to Eq. (7) yields

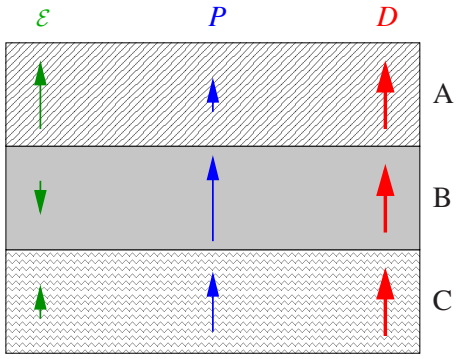

FIG. 1. (Color online) Sketch showing conservation of longitudinal component of displacement field D but not electric field $\mathcal{E}$ or polarization P, in an insulating superlattice composed of three dielectric constituents A, B, and C.

$$\bar{\varepsilon}(d)=\bar{\varepsilon}_{\mathrm{L}}(d)+N\bar{\varepsilon}_{\mathrm{b}}(d)+\bar{\varepsilon}_{\mathrm{R}}(d), \quad (15)$$

where $\bar{\varepsilon}_{\mathrm{bulk}}$ is the potential drop across a unit cell of the bulk insulator at a given value of d and $\bar{\varepsilon}_{\mathrm{L,R}}=dU_{\mathrm{L,R}}/dd$ contains the interface-specific information.

The potentials and the energies contain the same information, apart from a constant of integration, and one can choose to work with one or the other as a matter of practical convenience. Indeed, when analyzing the electrical properties of a capacitor, one is generally interested in energy *differences* between two different electrical states rather than in the total energy of the device. Therefore, the constant of integration that gets lost in going from Eq. (14) to Eq. (15) is not important for the scope of our discussion. Thus, we shall assume henceforth that $U(0)=0$, which also implies that the constant energies $\bar{U}_{\mathrm{L,R}}$ in Eq. (14) have been set to zero.

D. Decomposition of the interface contribution

1. Partial decomposition

Since $U(d)$ and $\bar{\varepsilon}(d)$ in Eqs. (14) and (15) can be obtained from supercell calculations while $U_{\mathrm{b}}(d)$ and $\bar{\varepsilon}_{\mathrm{b}}(d)$ can be obtained from bulk insulator calculations, it is straightforward to extract the quantities

$$U_{\mathrm{int}}(d)=U_{\mathrm{L}}(d)+U_{\mathrm{R}}(d) \quad (16)$$

and

$$\bar{\varepsilon}_{\mathrm{int}}(d)=\bar{\varepsilon}_{\mathrm{L}}(d)+\bar{\varepsilon}_{\mathrm{R}}(d) \quad (17)$$

representing the total impact of *both* electrodes on the electrical equation of state of the capacitor. Explicitly, we take

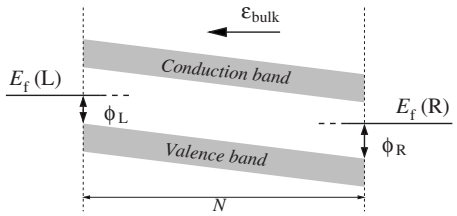

FIG. 2. Schematic model of the decomposition of the potential into bulk and interface contributions. An electron traveling from the L electrode to the R electrode experiences potential variations in $-\phi_L$, $N\bar{\varepsilon}_{bulk}$, and ϕ_R; the total variation is $\bar{\varepsilon}=E_f(R)-E_f(L)$.

$$\bar{\varepsilon}_{int}(d) = \bar{\varepsilon}_N(d) - N\bar{\varepsilon}_b(d). \tag{18}$$

Often, this is all that is needed, e.g., for modeling the polarization and dielectric response of a given device as a function of the oxide film thickness (we shall demonstrate this in our first application to $Pt/BaTiO_3/Pt$ capacitors). The number N of cells of insulating material should be kept small enough to avoid an undue computational burden while remaining large enough to decouple the two electrode interfaces so that the center of the oxide slab should behave like the bulk material within the same mechanical (in-plane strain) and electrical (d) boundary conditions.

2. Full decomposition

There are, however, situations in which it may be valuable to obtain the individual terms in Eq. (17), i.e., to define the individual interfacial potential steps $\bar{\varepsilon}_L$ and $\bar{\varepsilon}_R$ which occur at the left and right electrode interfaces, respectively. However, instead of using quantities defined as offsets of the average electrostatic potential across the interface, we find it more physical to use variables ϕ_L and ϕ_R that are the offsets of the metal Fermi levels $E_f(L)$ and $E_f(R)$ relative to the VBM just inside the insulator as illustrated in Fig. 2. With this choice, ϕ_L and ϕ_R are just the p-type Schottky barrier heights (SBH) at the metal/insulator interface. (It would be equally viable to adopt the CBM as the reference, corresponding to n-type Schottky barriers, but we do not do so here.) As long as both electrodes are made from the same material,[23] the total potential step is just $\bar{\varepsilon}=E_f(R)-E_f(L)$. This difference can be decomposed by following the hypothetical path in Fig. 2 of an electron traveling from the left electrode through the insulator and into the right electrode and we obtain

$$\bar{\varepsilon} = -\phi_L + N\bar{\varepsilon}_b + \phi_R. \tag{19}$$

In the remainder of this section, we make some of the above definitions more precise and discuss how in practice to extract accurate values of the SBH at a polarized metal/insulator interface. The main issue here is that, whenever $\bar{\varepsilon}_b$ is nonzero, the SBH is somewhat ill defined because the VBM does not have a well-defined asymptotic value deep in the oxide. (Instead, it varies linearly with depth, with a slope corresponding to the internal electric field $\mathcal{E}_b$). In the next few paragraphs, we propose a procedure that provides a reasonable yet sharp definition of ϕ_L and ϕ_R even when $\mathcal{E}_b \neq 0$.

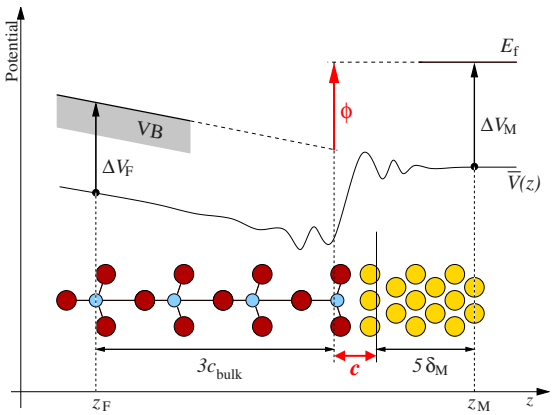

FIG. 3. (Color online) Illustration of proposed procedure for evaluating the p-type Schottky-barrier height ϕ at a perovskite/metal interface when a macroscopic field is present in the insulating layer. Small light blue (light gray) circles correspond to B-site cations, large red (dark gray) circles to oxygens, and large gold (light gray) circles to the metal electrode atoms.

For the moment we assume an interface configuration with the semi-infinite electrode at right and the film at left. The situation is sketched in Fig. 3, which also illustrates the following discussion. We first compute the planar average of the local electrostatic potential, $V_H(\mathbf{r})$, further convoluted with a Gaussian filter of width α to suppress the short-range oscillations

$$\bar{V}(d,z) = \frac{1}{\sqrt{\pi}\alpha S}\int V_H(d,\mathbf{r}')e^{-(z-z')^2/\alpha^2}d^3\mathbf{r}'. \tag{20}$$

Next, we identify two z coordinates on either side of the interface, z_F in the film and z_M in the metal. Both z_F and z_M must be located far enough from the interface that the short-range structural distortions related to interface bonding have already relaxed back to the regular bulklike spacings of the respective material (oxide film or metal electrode). As a further requirement, we impose that the interface-related perturbations in the local electrostatic potential $\bar{V}(z)$ (schematically indicated in the figure by the strong oscillations near the metal/film boundary) are also negligible in the neighborhood of both z_F and z_M. This implies that $\bar{V}(d,z)$ is a linear function near z_F with a finite slope given by the bulk internal field $\mathcal{E}_{bulk}(d)$, and $\bar{V}(d,z)$ is a constant near z_M. We generally find that three perovskite unit cells on the film side and five monolayers on the electrode side are sufficient for both requirements [on the structure and $\bar{V}(z)$] to be satisfied accurately. We therefore set z_F as the z coordinate of the fourth B-site cation in the film (numbering as 1 the B cation which lies adjacent to the interface) and z_M as the z coordinate of the sixth metallic layer in the electrode.

Now, using these two reference points in the lattice, we extract $\bar{V}(d,z_M)$ and $\bar{V}(d,z_F)$, which are indicated in the figure as black circles. On the film side, we use $\bar{V}(d,z_F)$ to estimate the VBM at the interface

$$E_{\mathrm{VBM}}(d) = \bar{V}(d,z_F) + \Delta V_F(d) + 3\bar{\varepsilon}_{\mathrm{bulk}}(d), \tag{21}$$

where $\Delta V_F(d)$ is the relative position of the VBM to the average electrostatic potential in the bulk (techniques for calculating this are detailed in Sec. V C). On the metal side we compute the Fermi energy as

$$E_{\mathrm{f}}(d) = \bar{V}(d,z_M) + \Delta V_M, \tag{22}$$

where ΔV_M (independent of d) is again a bulk property, i.e., the relative position of the Fermi level to the average electrostatic potential of the metal. Finally, we define the p-type Schottky barrier as

$$\phi(d) = E_{\mathrm{f}}(d) - E_{\mathrm{VBM}}(d). \tag{23}$$

It is easy to verify that this definition reduces to the standard technique for calculating Schottky barriers at metal/semiconductor interfaces[24] whenever the macroscopic field in the oxide vanishes. Note that the above construction provides, as a byproduct, structural parameters that are relevant for accessing the piezoelectric properties of the device. In particular, starting from the same z_F and z_M, we define an interfacial expansion

$$c(d) = |z_M - z_F| - Nc_{\mathrm{bulk}}(d) - 5\delta_M, \tag{24}$$

where δ_M is the bulk interlayer distance of the metal (see Fig. 3).

Note that, while there is an intrinsic arbitrariness in the definition of $\phi(d)$ and $c(d)$ (several choices are possible for z_F), the arbitrariness always cancels out in the final equation of state of the entire capacitor because of the way these functions are always summed up in pairs (a capacitor always has two electrodes). We also note that these functions, by construction, transform properly under spatial inversion, so that for a capacitor having a centrosymmetric reference structure, we have $\phi_{\mathrm{R}}(d)=\phi_{\mathrm{L}}(-d)$ and $c_{\mathrm{R}}(d)=c_{\mathrm{L}}(-d)$.

3. ΔV_F and ΔV_M

ΔV_M can be calculated with high precision for the bulk metal by extracting the Fermi level and the average electrostatic potential from the structural and electronic ground state. To define $\Delta V_F(d)$ we start from a constrained-D calculation of the bulk oxide. Since a macroscopic electric field is generally present, the values of both the VBM and the average electrostatic potential are not directly obvious from the eigenvalue spectrum (strictly speaking, the energy eigenvalues themselves are ill defined). The effect of an electric field is to induce a linear ramp in the electrostatic potential and a corresponding linear "tilting" of the energy bands. For a given value of the macroscopic electric displacement, the VBM and the average electrostatic potential will therefore have the same linear z dependence and the difference $\Delta V_F = V_{\mathrm{VBM}}(z) - V_H(z)$ will be independent of z. In practice we compute ΔV_F by first relaxing the structural and electronic degrees of freedom in the finite field, using the usual convention that the electrons feel a periodic electrostatic potential having zero unit-cell average, plus a coupling to the field through the Berry-phase polarization. ΔV_F is then obtained by diagonalizing the *zero-field* Hamiltonian operator in the subspace spanned by the wave functions, which form the "ground state" of the finite-field calculation and finding its maximum over the wave vectors in the Brillouin zone.

Note that this procedure is to some extent arbitrary and it is certainly possible to adopt alternative strategies. Whatever choice is made, the only important requirement is to have a well-defined reference energy in the insulating lattice as a function of D; the arbitrariness in the specifics of this choice cancel out anyway when we consider a complete capacitor heterostructure.

E. Computational parameters

Our calculations are performed within the local-density approximation of density-functional theory and the projector-augmented-wave method[25] as implemented in an "in-house" code. We used a plane-wave basis cut-off energy of 40 Ry in Sec. III and of 80 Ry in Sec. IV; the higher value in the latter case is intended to minimize the Pulay error in the stress and the numerical noise in the energies which are due to the discrete nature of the basis set.[26] In all cases we fix the in-plane lattice parameter to a constant value and we enforce a tetragonal $P4mm$ symmetry constraint; the out-of-plane lattice parameter, as well as the internal coordinates, are allowed to relax fully. The Brillouin-zone integrations of the capacitor heterostructures are performed with a $6\times6\times1$ mesh, where $k_z=0$ and the grid is shifted in-plane according to the Monkhorst-Pack[27] prescription for two-dimensional sampling; the Gaussian smearing energy is set to 0.15 eV. In the bulk calculations we use a $6\times6\times6$ Monkhorst-Pack mesh, which is sufficient to converge both the structural and the dielectric response of the crystal to an accuracy comparable to that of the capacitor calculations. To relax the structure (both internal coordinates and the out-of-plane strain) at each d value we use a steepest-descent approach, optimally preconditioned by inverting the force-constant matrix and the elastic constant calculated in the centrosymmetric $d=0$ configuration. Generally, five to ten iterations were sufficient to relax the geometries to a stringent convergence threshold for both forces (10^{-3} eV/Å) and stresses (10 MPa). (To ensure excellent accuracy of the calculated energies and potentials, we further enforce a threshold of 1% convergence in the internal electric field.)

Correcting for the Pulay error in the stress is crucial to accurately model the strain-polarization coupling effects discussed in this work. We use a technique similar in spirit to the prescription of Ref. 26. In particular, we define the corrected stress σ_{ij} as

$$\sigma_{ij} = \sigma_{ij}^0 + \frac{C\delta_{ij}}{\Omega}, \tag{25}$$

where σ_{ij}^0 is the calculated stress tensor (analytical derivative at fixed number of plane waves), Ω is the cell volume, and C is a constant (dependent on the cell stoichiometry and plane-wave cut off). To evaluate C several techniques are possible. A possible strategy is to fit the dependence of the total energy on the plane-wave cut off as discussed in Ref. 26. In our calculations, we infer C by imposing $\sigma_{ij}=0$ in Eq. (25) for a particular configuration of a given system that has been

structurally relaxed using a different technique (e.g., a Murnaghan fit to the energy/volume curve).

III. RESULTS: Pt/$BaTiO_3$/Pt CAPACITORS

We start by analyzing the polar ground state at zero bias of 7-, 5-, 3-, 2-, and 1-unit-cell-thick $BaTiO_3$ films with compositionally symmetric (the overall spatial symmetry is broken upon ferroelectric off-centering) BaO terminations and Pt electrodes. (N-unit-cell capacitors are actually "$N+1/2$" perovskite cells thick; e.g., $N=1$ means Pt-BaO-TiO_2-BaO-Pt.) The Pt electrodes are modeled by a nine-layer Pt slab in periodic boundary conditions. We fix the in-plane lattice constant[28] to $a_0=7.276$ a.u., the theoretical equilibrium value for cubic $SrTiO_3$ (STO), and we allow the out-of-plane lattice parameter of the tetragonal supercell, as well as the internal coordinates, to relax fully. We shall start by discussing our motivation for choosing this system. We shall proceed then to present our results for the structural and dielectric properties at zero bias. Finally, we shall use our constrained-D techniques to study the electrical behavior of the system as a function of bias and BTO thickness.

A. Motivation

Our goals in this section are threefold. First, we shall introduce our methods for computing the macroscopic polarization in short-circuited ferroelectric capacitors, separating the different contributions that we discussed in Sec. II A 2. Second, we shall analyze the structural and electrical properties as a function of the thickness of the short-circuited film, identifying those aspects that are common to ferroelectric single-crystal $BaTiO_3$, and those that depart from the bulk behavior. Third, we shall demonstrate with a quantitative model that even these thickness-dependent perturbations can be understood in terms of the bulk properties of $BaTiO_3$, once the interface contribution is properly taken into account. This analysis is primarily aimed at verifying in practice our locality principle, which allows us to separate the equation of state of a capacitor into two interface contributions and a bulklike term. We shall show that, in the case of Pt/$BaTiO_3$/Pt, this separation works with excellent accuracy down to a thickness of only two $BaTiO_3$ unit cells.

The choice of Pt and $BaTiO_3$, and more specifically of the BaO-terminated interface, is motivated by the recent prediction[7] of a chemical-bonding mechanism that enhances the ferroelectricity of the film beyond the bulk $BaTiO_3$ value. Because of this effect, it was found that Pt/$BaTiO_3$/Pt capacitors remain ferroelectric down to a single unit cell of $BaTiO_3$, i.e., there is no critical thickness below which the polar instability is suppressed. Given the practical interest in overcoming the usually deleterious size effects in ferroelectric devices, the Pt/$BaTiO_3$/Pt system is therefore an appealing test case for the present study. We warn the reader, however, that the above-mentioned features of the Pt/$BaTiO_3$/Pt system are to some extent anomalous, i.e., they depart from the usual understanding of depolarizing effects in thin-film ferroelectrics. For this reason, the results presented in this section should not be understood as an example of the most typical ferroelectric capacitor. Instead, this application to Pt/$BaTiO_3$/Pt illustrates how the general strategy developed in this work (free from *a priori* assumptions) is particularly effective at capturing the peculiar physics of a highly nonstandard case. The TiO_2-terminated interface of $BaTiO_3$ with Pt would perhaps have provided a more "regular" example, which, in principle, could have allowed us to trace a closer link with earlier first-principles and phenomenological results. However, this system is inappropriate because it suffers from the band-alignment issues mentioned in Ref. 4. In particular, we find that the TiO_2-terminated $BaTiO_3$/Pt interface has charge-spillage problems already when the capacitor is in the paraelectric reference structure, thwarting attempts at defining a polarization or even introducing an external bias potential. In Sec. IV we consider a different ferroelectric/electrode combination ($BaZrO_3$/Au) whose BO_2-type interface is free from band-alignment problems; in that case we are able to compare two different interface types and discuss the differences between a "standard" and a "nonstandard" case.

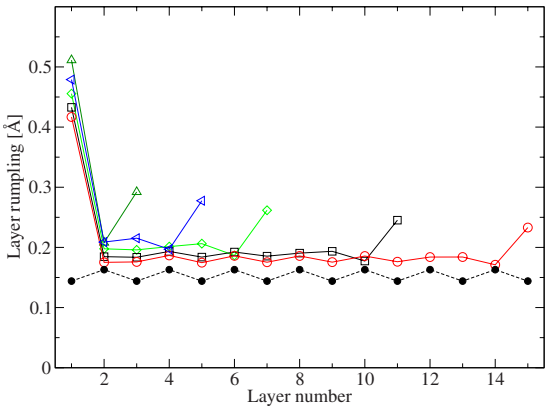

FIG. 4. (Color online) Layer rumplings, defined as cation displacements relative to oxygens, for oxide layers in relaxed short-circuited Pt/$BaTiO_3$/Pt capacitors containing seven (circles), five (squares), three (diamonds), two (left triangles), or one (up triangles) perovskite unit cells. Odd and even layer numbers refer to BaO and TiO_2 layers, respectively, with Layer 1 being the BaO layer that is chemically bonded to the Pt. Bulk values are shown for comparison as filled symbols connected by dashed lines. The polarization is along $+\hat{z}$.

B. Structural and dielectric properties at zero bias

Here we shall present our results starting from a comparative analysis of the relaxed atomic positions in our short-circuited Pt/$BaTiO_3$/Pt capacitors; then we shall gradually introduce the ingredients that enter the definition of the polarization and its coupling to an external field.

1. Structural properties

We plot in Fig. 4 our calculated results for the layer rumplings of the relaxed capacitors at zero bias, defined as the cation displacement relative to the oxygens in the same oxide layer; in the same figure we report the calculated rumpling values for bulk $BaTiO_3$ as a comparison. The most striking

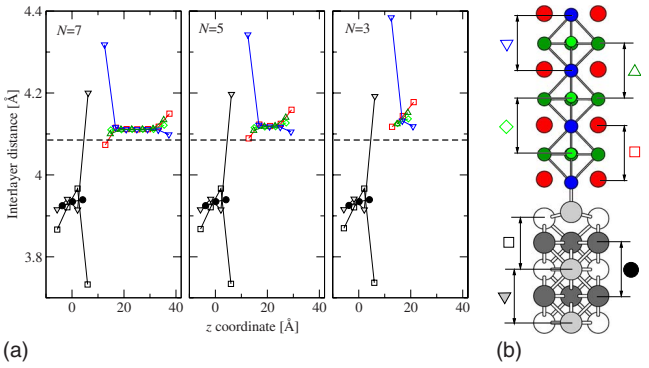

FIG. 5. (Color online) Relaxed interlayer distances of short-circuited $Pt/BaTiO_3/Pt$ capacitors with oxide thickness of 7, 5, and 3 unit cells and nine Pt layers. Black (left) and colored (right) symbols/lines correspond to Pt and oxide layers, respectively. Vertical axis indicates distances between neighboring cations belonging to the same sublattice (see right panel); horizontal axis is the midpoint coordinate. Dashed line indicates the calculated equilibrium out-of-plane lattice parameter of bulk $BaTiO_3$ strained to the STO in-plane lattice constant. The code for the symbols and colors is schematically explained in the right panel, where the relaxed structure of the bottom interface (located at $z \simeq 10$ Å) is shown. Each symbol and color corresponds to a different sublattice: Pt1 (downward triangles with light gray filling), Pt2 (empty black squares), Pt3 (black circles), Ba (red/dark gray empty squares), Ti (green/light gray diamonds), O1 (blue/dark gray empty downward triangles), and O2 (dark green/dark gray upward triangles).

feature at all thicknesses is the strong bucking of layer 1, which is the BaO layer directly in contact with the Pt surface on the negatively polarized end of the films. (The BaO buckling is also enhanced at the positively polarized end but the effect there is significantly smaller.) Quite interestingly, the rumplings of all the films are systematically larger than the bulk values; furthermore, the enhancement in the structural distortions becomes more important in thinner films. This is unexpected as the depolarizing effect is known to suppress polarization and symmetry-breaking distortions in the ultrathin limit. The mechanism leading to such an enhancement is related to the interfacial chemical-bonding effect discussed in Ref. 7; we shall clarify this point in the following.

In Fig. 5 we plot the interlayer distances between ions belonging to the same sublattice, focusing here on the 3-, 5-, and 7-cell-thick capacitors only. (Atoms are grouped in different sublattices according to their chemical identity. Pt and O atoms are further split into three and two sublattices, respectively, as shown schematically in the right panel of Fig. 5.) The atomic layers closest to the interface undergo strong distortions, both on the electrode and on the insulator side. The largest effects are located again on the negatively polarized end of the film. Here, the surface Pt atoms and the BaO ions strongly buckle with the overall effect of reducing the Pt-O distance (which ranges from 2.01 to 2.04 Å in the capacitors considered) and increasing the Ba-Pt distance (~2.9 Å). These features are consistent with the oxygen binding chemically to the Pt surface while the Ba atom repels the Pt atom that lies directly underneath. Such a picture was proposed, from an analysis of the centrosymmetric reference structure, in Ref. 7; here we can see its impact on the properties of the fully polarized state of the film. At the positively polarized end of the film, the structural distortions of the Pt surface are relatively minor and the oxide film does not appear to be chemically interacting with the electrode; the Pt-O distances in all capacitors are larger than 3.3 Å and the metal-oxide bonding appears to be of purely electrostatic nature. Two monolayers away from the interface, the interlayer distances of the BTO film converge to a uniform value, which can be understood as the relaxed strain state of the film in the capacitor heterostructure. In all cases this value is larger than in the equilibrium value of the strained bulk, which is indicated in the same figure as a dashed horizontal line. (The bulk out-of-plane strain was calculated by imposing the same in-plane strain as in the capacitor calculations; therefore, the effect shown in Fig. 5 is *not* of mechanical origin.) Remarkably, the tetragonality of the film increases for thinner capacitors. Since ferroelectrics have a strong coupling between polarization and strain, this provides additional evidence to the enhancement of polarity we already pointed out earlier while discussing the layer rumplings.

Note that such a strong coupling makes the results very sensitive to the accuracy in the relaxation of the out-of-plane lattice constant. To this end, it is crucial to properly take into account the effect of the Pulay stress as explained in Sec. II E. In order to check that this procedure was effective, we monitored in all capacitors the interlayer distance in the center of the Pt slab, i.e., the black circle at $z=0$ in the three panels of Fig. 5. The maximum deviation in this value was less than 10^{-3} Å, confirming that our structural relaxations are very well converged.

In the next section we shall investigate the electrical properties of the Pt/BTO/Pt capacitors and demonstrate the ferroelectric nature of the enhanced structural distortions discussed above.

2. Polarization and electrical properties

Our goal now is to evaluate the macroscopic polarization of the capacitor heterostructures discussed in the previous section. Since all the capacitors are relaxed within standard short-circuit electrical boundary conditions, the macroscopic electric field is zero and the polarization is equal to the electric-displacement field D.

First we assess the level of accuracy we can expect for the value of the polarization computed according to the technique discussed in the methods section. To that end, we analyze the planar-averaged conduction charge $\rho_{\mathrm{cond}}(z)$ as defined in Eq. (4) by setting the width of the middle energy window $\delta=0.5$ eV. Given the Gaussian smearing of $\sigma=0.15$ eV, $[E_f-\delta, E_f+\delta]$ encompasses all partially occupied states within an occupancy threshold of 10^{-6}. In other words, at the bottom of the window the smearing function $f(E_f-\delta)$ is equal to $1-10^{-6}$ while at the top $f(E_f+\delta)=10^{-6}$. Recall that all states lying higher in energy are discarded; all states lying below this window are treated as fully occupied and transformed into Wannier functions as we shall discuss shortly.

To define the dipole moment of $\rho_{\mathrm{cond}}(z)$ it is essential that this function be small in the middle of the insulating region. Whenever the film is not thick enough for $\rho_{\mathrm{cond}}(z)$ to decay

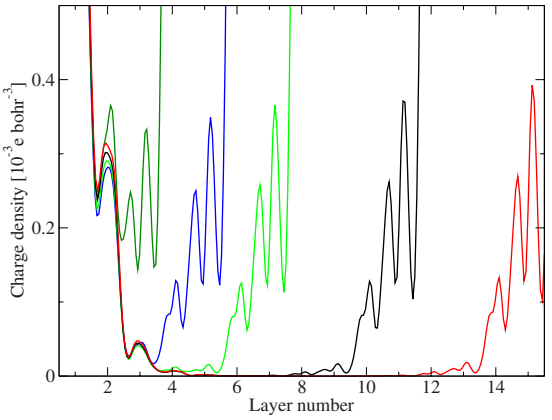

FIG. 6. (Color online) Conduction-charge density $\rho_{\mathrm{cond}}(z)$ [Eq. (4)] for five $Pt/BaTiO_3/Pt$ capacitors of Fig. 4.

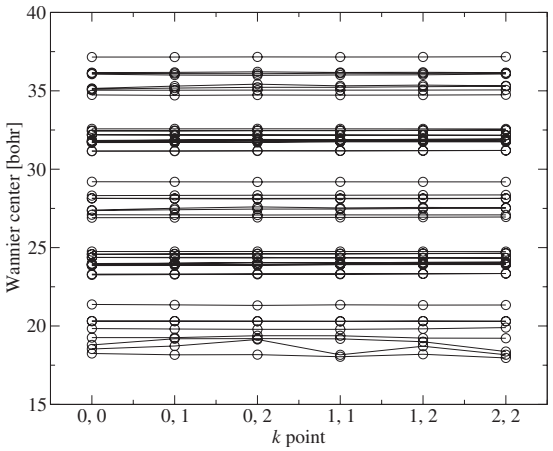

FIG. 7. Wannier centers in the 2-unit-cell $BaTiO_3$ film as a function of in-plane k point in the irreducible 2D Brillouin zone, labeled as (i,j) according to $\mathbf{k}_{\parallel}=(i+1/2,j+1/2)/6$. Second and fourth groups of centers correspond to TiO_2 layers; others are BaO, of which the first and fifth are in contact with Pt. P points up.

to zero, this introduces an error in the definition of the macroscopic P which can be roughly estimated by

$$\Delta P \sim \rho_{\mathrm{cond}}(L/2)\,\delta z. \tag{26}$$

Here $L/2$ corresponds to the center of the insulating film and δz is a length that takes into account the arbitrariness in the positioning of the discontinuity of the sawtooth function used to define the dipole moment of ρ_{cond}. We shall assume δz to be half an oxide layer or 2 bohr units.

To give an idea of how the conduction charge decays in the oxide films, we plot in Fig. 6 the calculated $\rho_{\mathrm{cond}}(z)$ in the five structures considered. While the thinnest capacitor (1-cell-thick, leftmost curve in the graph) is clearly metallic, in all other structures the conduction charge decays almost to zero in the central oxide layer. The estimated accuracy using the above formula is on the order of 0.5 $\mu C/cm^2$ for the 2-cell-thick capacitor, decreases by a factor of 3–4 for the 3-cell-thick capacitor and further decreases at an exponential rate of 1 order of magnitude per each two more unit cells added. This means that, at a thickness of 5 unit cells, the estimated error is on the order of 0.01 $\mu C/cm^2$, i.e., already smaller than the overall numerical accuracy of our calculations. In the remainder of this section, therefore, we shall drop the one-cell structure from our discussion and focus on the remaining four structures, where the value of the macroscopic P can be accurately defined.

The fully occupied states are transformed, separately for each k point, by means of the parallel transport algorithm.[17] This yields a set of orthonormal orbitals which sum up to the same charge density and are maximally localized along the polarization direction (their Bloch-type character is preserved in plane). Note that the actual number of states differs for each k point. Therefore, when performing the Brillouin-zone averages of the polarization, particular care must be taken in order not to introduce by mistake a fraction of the quantum of polarization into the final value. In order to ensure that this issue is properly taken care of, it is useful to analyze how the Wannier centers distribute in space for each k point. Upon visual inspection, we find that the Wannier centers are characterized by a significant degree of disorder in the metallic region as might be expected by recalling that the band structure of the metallic slab is not constituted by full energy bands and in our algorithm it is abruptly "cut" at $E_f-\delta$. Conversely, in the insulating region, we find that the Wannier centers cluster nicely around the oxide layers, analogously to what happens in purely insulating superlattices;[19] to demonstrate such a behavior we plot in Fig. 7 the calculated Wannier centers for the two-cell capacitor. The total number of orbitals shown in Fig. 7 for each k point matches exactly the "nominal" number of valence orbitals of the oxide ions. This means that the oxide film can be identified as a charge-neutral and spatially confined subsystem, whose dipole moment can be computed with high accuracy and potential issues with the quantum of polarization are therefore completely avoided. (Note the increased k-space dispersion in the Wannier centers associated with the bottom BaO layer; this is due to the strong perturbation induced by chemical bonding with Pt.)

By combining the ingredients discussed in the above paragraphs, we now compute the electric displacement D of the films, which is plotted as a function of film thickness in Fig. 8. In the thickest seven-layer film $D=46.1$ $\mu C/cm^2$, which is 17% larger than the spontaneous polarization of bulk BTO within the same mechanical boundary conditions (shown as a horizontal dashed line in the same plot). This indicates that the electrical boundary conditions induce an *enhancement* in the polarity of the film; this is unlike the vast majority of cases, where generally a suppression of P due to depolarizing effects is observed. The enhancement in P is due to the chemical bonding at the negatively polarized end of the film to the Pt surface. Such an effect was discussed for the centrosymmetric geometry in Ref. 7; the present study of the fully relaxed capacitors in short circuit demonstrates that the effect persists in the polar structure. In fact an analysis of the local electrostatic potential shows that there is, instead of the usual depolarizing field (which would oppose the spontaneous P), a strong "polarizing" field; its magnitude is in excess of 200 MV/m and drives the film significantly more polar than the bulk.

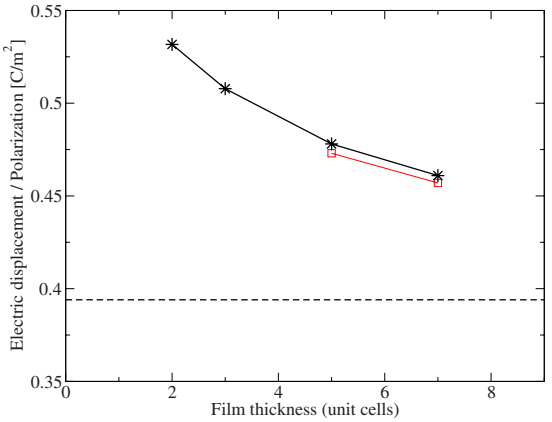

FIG. 8. (Color online) Calculated values of the electric displacement field (or surface density of free charge stored on the plates) for short-circuited $BaTiO_3$ capacitors (black solid line and star symbols). The calculated bulk spontaneous polarization of $BaTiO_3$ at the $SrTiO_3$ in-plane lattice parameter is shown as a horizontal dashed line. Red (gray) squares are the values of the macroscopic polarization P_{mac} of the 5- and 7-unit-cell capacitors as defined in Eq. (27).

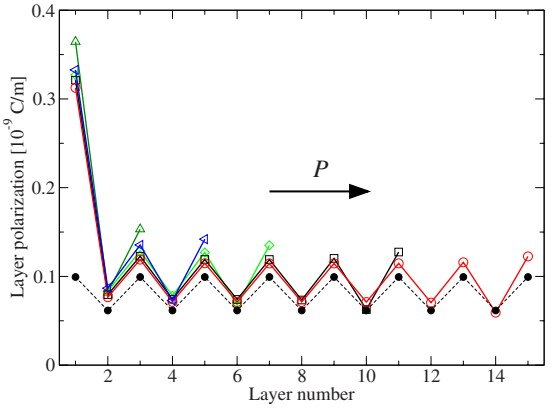

FIG. 9. (Color online) Calculated Wannier-based layer polarizations for the capacitors discussed in the text. Even-numbered layers are TiO_2; odd layers are BaO. Bulk values are reported for comparison as filled circles connected by dashed lines.

In such a "negative dead-layer" regime one would expect thinner films to be even more polar. This is nicely confirmed by our results, shown in Fig. 8, where the polarization enhancement attains values as large as 35% in the 2-cell-thick capacitor; also the tetragonal ratio and the internal electric fields (not shown) steadily increase with decreasing thickness as expected from the above qualitative arguments.

3. Layer polarizations and macroscopic polarization

While it is not a necessary step to computing the macroscopic P, it is nonetheless interesting to push further the analogy to insulating superlattices and compute the LP as defined in Ref. 19. This involves grouping the Wannier centers of Fig. 7 into the separate clusters corresponding to the individual oxide layers, which are obvious from the plot, and computing the individual dipole moment p_j per surface unit (see methods section). We plot in Fig. 9 the results for the Wannier-based layer polarizations. In all cases the dipole moment of the first BaO layer is about three times larger than the LP values in the rest of the films. This qualitatively reflects the strong structural distortion due to the chemical interaction with the Pt surface, which was discussed in the previous section. Otherwise, the LPs display qualitative features which are remarkably similar to bulk $BaTiO_3$. In particular, the LP of both layer types (BaO and TiO_2) have the same positive sign (consistent with the positive displacement of all cations with respect to the O sublattice) with the LPs of the BaO layers systematically larger than the TiO_2 values (approximately by a factor of 1.6). Note that in all cases the LPs are larger than the corresponding bulk values and uniformly increase as the film becomes thinner. This confirms that the enhanced structural distortions discussed in the previous section correspond indeed to an enhanced polarization of the films.

It is interesting to note that the LPs converge rather quickly to a uniform bulklike sawtooth pattern two or three oxide layers away from the interface, which indicates that the perturbations induced by the electrode are rather local. This contrasts sharply with the picture proposed in a recent work[11] for the same system. We defer a detailed discussion of this issue to Sec. V.

The local LP values in the middle of the ferroelectric, p_{BaO} and p_{TiO_2}, together with the average out-of-plane strain c_{avg} inferred from the data of Fig. 5, provide an accurate estimate of the macroscopic P inside the film as

$$P_{film} = \frac{e}{c_{avg}}(p_{BaO} + p_{TiO_2}). \tag{27}$$

We plot P_{film} of the 5- and 7-unit-cell capacitors as square symbols in Fig. 8; here P_{film} can be directly compared to the calculated values of the electric displacement D. First, the values of D and P_{film} are very close as can be expected from their relationship (in SI units) $D=\epsilon_0\mathcal{E}_{film}+P_{film}$: indeed, $\epsilon_0\mathcal{E} \ll P$ in typical ferroelectrics. Next, the fact that D is slightly larger than P is consistent with the electric field's being collinear with P in the capacitors considered here, i.e., the interface induces a polarizing effect instead of a depolarizing one as we already discussed extensively.

Note that the electric field $\mathcal{E}_{film}$, as P_{film}, is the macroscopically and planar-averaged value of $\mathcal{E}(x)$ inside the film and far from the interfaces. Therefore, we identify $\mathcal{E}_{film}$ and P_{film} as, respectively, the *internal field* and the polarization that are typically discussed in Landau-Ginzburg models of thin-film ferroelectrics. As will become clearer in the following sections, the relationship between $\mathcal{E}_{film}$, P_{film}, and D is an intrinsic property of *bulk* $BaTiO_3$, and does not depend on the interfaces, electrical boundary conditions or applied bias potential. This point is crucial to the development of our modeling strategies and therefore we consider the above definitions of P_{film} and $\mathcal{E}_{film}$ to be very convenient. Other authors[29,30] defined P by averaging the dipoles over the whole volume of the film, including the interface region. Such a choice is less convenient for modeling as (i) it does not provide a clear separation between bulk and interface effects and (ii) it introduces a degree of arbitrariness as the

"bound" dipoles near the interface are strongly mixed with the metallic free carriers.

Summarizing the above results, we have shown that, in thin-film capacitor configurations with Pt electrodes, BaO-terminated $BaTiO_3$ films display many features that are typical of a bulklike crystal within the same mechanical boundary conditions (in-plane strain). However, in addition to these similarities, there are also a few remarkable departures from the bulk behavior that are fully consistent with an interface-induced polarization enhancement. The effect is stronger in thinner films, which is at odds with the common belief that realistic electrodes would systematically induce a polarization suppression due to imperfect screening.

In the following we shall use the constrained-D method to understand the origin of this effect. In particular, we shall demonstrate that the locality principle is restored once the long-range electrostatic interactions are properly rationalized. In particular, we shall show that a simple model of this system with full *ab initio* accuracy can be constructed in terms of the electrical properties of bulk $BaTiO_3$ and of the BaO-terminated Pt/BTO interface.

C. Electrical equation of state

In order to model the electrical behavior of the Pt/BTO capacitors considered in this work, we now use the fixed-D method to sample the equation of state of the 5-cell-thick capacitor; this is the thinnest one in which ρ_{cond} is essentially zero in the middle of the oxide film, which ensures a high level of accuracy. For the scope of the present discussion, it is enough to restrict our investigation to a range of D that encompasses the equilibrium values calculated for different thicknesses in short circuit, i.e., $0.4e<d<0.5e$. Subsequently, we shall show how this information can be combined with the bulk equation of state to predict the properties of capacitors of arbitrary thickness. We shall start by calculating the electrical equation of state of bulk BTO.

1. *Bulk* $BaTiO_3$

As in the capacitor structures, we fix the in-plane lattice constant to $a_0=7.276$ a.u., the theoretical equilibrium value for cubic $SrTiO_3$ and we let the out-of-plane lattice parameter as well as the internal coordinates of the five-atom tetragonal unit cell, relax as a function of the reduced electric displacement d. We use twelve values of d, equally spaced between $d=0.0$ and $d=0.55$. We extract from the calculation the values of the potential and the c lattice parameter for every value of d; then we use splines to interpolate these values and we finally integrate the potential to recover the internal energy U. The results are plotted in Fig. 10. Note the perfect match between the values of U calculated *ab initio* (plus symbols) with the integrated potential (solid black curve); such a good match is a consequence of accurately compensating the Pulay stress with a fictitious constant negative pressure of $\pi=-2.61$ GPa. The Pulay error is high (due to the relatively low plane-wave cutoff of 40 Ry) and neglecting it would produce significant errors; with this simple correction, the numerical values are highly accurate.

The relaxed ferroelectric ground state ($\bar{\varepsilon}=0$) is at $d_0=0.364$, which corresponds to $P=39.4$ $\mu\mathrm{C/cm^2}$, an energy

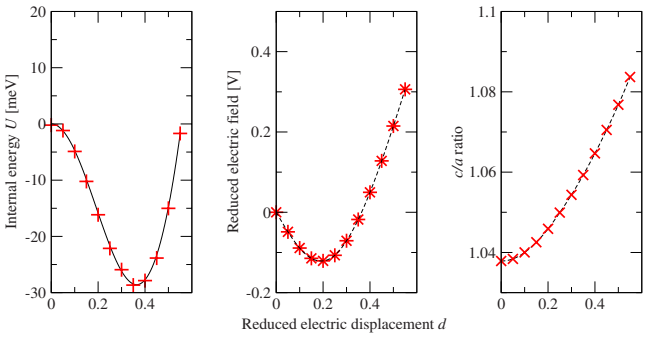

FIG. 10. (Color online) Internal energy, reduced electric field, and c/a ratio vs reduced displacement field (in units of e) for coherently strained bulk $BaTiO_3$. *Ab initio* data are shown as symbols; dashed curves in the middle and right panels are spline interpolations; and continuous curve in the left panel is the numerical integral of the spline in the middle panel.

$\Delta U=-28.6$ meV/cell, and $c/a=1.061$. Note that this is considerably larger than the value, $c/a=1.038$, in the strained centrosymmetric geometry. We can understand the c/a ratio of the epitaxially constrained ferroelectric phase as a result of two distinct contributing factors. One effect comes from the elastic properties (Poisson ratio) of the centrosymmetric crystal; straining $BaTiO_3$ to the $SrTiO_3$ lattice constant (-2.1%) produces a tetragonality of $c/a=1.038$ even in the absence of a polar distortion. The second effect, related to polarization-strain coupling, bring this value to $c/a=1.061$ once the unstable "soft" mode is condensed. For more details about the relationship between polarity and epitaxial strain we direct the reader to Ref. 31.

2. *Capacitor structures*

We shall write the electrical equation of state of the 5-unit-cell capacitor as $\bar{\varepsilon}_5(d)$, the d-dependent reduced electric field. Since we already have one data point from the calculation in short circuit ($d=0.442e$, $\bar{\varepsilon}=0$) and we expect the potential to be a rather smooth function of d, it is likely that two additional points lying at the extremes of the interval will be enough for constructing our model. Therefore, we repeat the calculation of the 5-cell capacitor twice with d set to $0.4e$ and $0.5e$, respectively. (In both cases the ionic positions and out-of-plane lattice parameter are relaxed to the same convergence thresholds used in the zero-field cases.) The smoothness of the potential is confirmed by our results, plotted as black circles in Fig. 11, which lie almost on a straight line.

To account for the small curvature, we interpolate the points with a second-order polynomial expanded around the spontaneous reduced displacement d_0 of the bulk. To establish notation, we do this first for a simple bulk crystal. Recalling that internal energies are related to the reduced electric fields by Eq. (7), $\bar{\varepsilon}(d)=dU/dd$ and anticipating an expansion of the internal energy up to third order in $d-d_0$

$$U_{\mathrm{b}}(d)=A_0^{\mathrm{b}}+A_1^{\mathrm{b}}(d-d_0)+\frac{A_2^{\mathrm{b}}}{2}(d-d_0)^2+\frac{A_3^{\mathrm{b}}}{3!}(d-d_0)^3, \tag{28}$$

we expand $\bar{\varepsilon}_{\mathrm{b}}(d)$ as

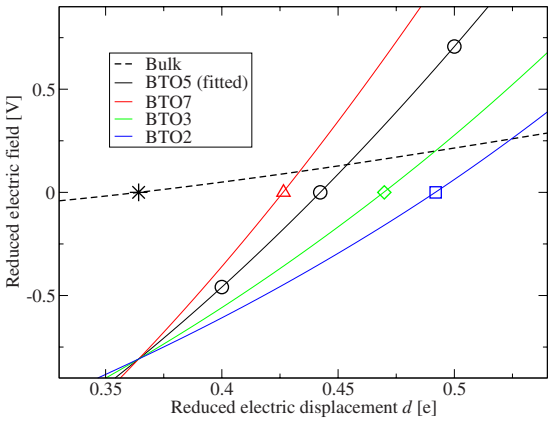

FIG. 11. (Color online) Calculated values of reduced electric field $\bar{\varepsilon}$ as a function of d in capacitors of various thicknesses (empty symbols). Solid lines correspond to the first-principles derived model described in the text. Dashed line is the calculated bulk equation of state (from middle panel of Fig. 10), which corresponds to the potential drop across a single bulk unit cell. Star corresponds to the relaxed ferroelectric state of the strained bulk crystal.

$$\bar{\varepsilon}_{\mathrm{b}}(d) = A_1^{\mathrm{b}} + A_2^{\mathrm{b}}(d-d_0) + \frac{A_3^{\mathrm{b}}}{2}(d-d_0)^2. \tag{29}$$

(Note that the expansion is carried out about the spontaneous displacement d_0 of the bulk so that A_1^{b} vanishes by construction.) We then carry out similar expansions for each N-cell capacitor, e.g., for $N=5$

$$U_5(d) = A_0^{(5)} + A_1^{(5)}(d-d_0) + \frac{A_2^{(5)}}{2}(d-d_0)^2 + \frac{A_3^{(5)}}{3!}(d-d_0)^3 \tag{30}$$

and

$$\bar{\varepsilon}_5(d) = A_1^{(5)} + A_2^{(5)}(d-d_0) + \frac{A_3^{(5)}}{2}(d-d_0)^2. \tag{31}$$

The fitted bulk expansion parameters A_n^{b} and the interface parameters defined via

$$A_n^I = A_n^{(5)} - 5A_n^{\mathrm{b}} \tag{32}$$

are reported in Table I.

TABLE I. Values, in atomic units, of the expansion coefficients used to model the bulk and interface contributions to the electrical equation of state, Eqs. (28), (29), (36), and (37), and to the elastic equation of state, Eqs. (40) and (43).

	Electrical EOS		Elastic EOS	
n	Bulk A_n^{b}	Interface A_n^I	Bulk c_n^{b}	Interface c_n^I
0	−0.0011	−0.0105	7.719	7.124
1	0	−0.0296	0.764	1.894
2	0.0501	0.0895	0.704	−3.745
3	0.0589	0.2245		

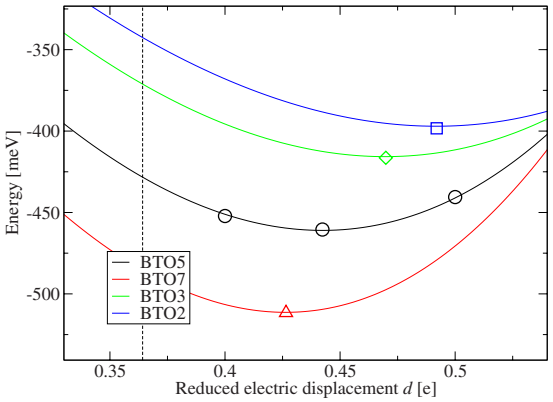

FIG. 12. (Color online) Calculated energies, relative to corresponding paraelectric state, for BTO capacitors of various thicknesses and polarization states (symbols). Solid curves correspond to the model discussed in the text. Vertical dashed line indicates the spontaneous polarization of bulk $BaTiO_3$.

Focusing first on Eq. (31) for the 5-cell-thick capacitor, the fitted $\bar{\varepsilon}_5(d)$ is shown as the solid black line passing through the circles in Fig. 11. Using this together with the bulk information encoded in Eq. (29), we can then *predict* the equations of state for thinner or thicker capacitors according to the formula

$$\bar{\varepsilon}_N(d) = (N-5)\bar{\varepsilon}_{\mathrm{b}}(d) + \bar{\varepsilon}_5(d). \tag{33}$$

Setting N to 2, 3, and 7 we obtain the colored solid curves in Fig. 11. The intersection of each curve with the $\bar{\varepsilon}=0$ axis yields a well-defined value of d, which is the predicted polarization state of a capacitor with thickness N, and can be directly compared to the first-principles data already in hand. To that end, we take the d values from Fig. 8 and plot them as colored symbols on the $\bar{\varepsilon}=0$ axis of Fig. 11. The agreement between the first-principles points and the model predictions is extraordinarily good (discrepancies are smaller than 0.1%). Surprisingly, this holds true even for the thinnest (2-cell) capacitor, where one would expect the estimation of d to be less accurate (see previous sections). Also, apart from purely technical issues in defining d, one might expect the properties of such a thin layer of oxide to depart somewhat from what is calculated in thicker capacitors. The accuracy of our model in this thickness regime is indeed encouraging and indicates that our methods for accessing the interfacial electrical properties are able to predict, with full first-principles accuracy, the behavior of a wide range of systems.

To further confirm the internal consistency of our model, we perform a similar analysis for the energetics of the capacitors. Let $U_N(d)$ be the difference in internal energy, for a given thickness N, between the state at specified d and the paraelectric structure at $d=0$. We plot in Fig. 12 the three values of $U_5(d)$ (black circles) that we extracted for the 5-cell capacitor from the same calculations described above. Expanding in $d-d_0$ according to Eq. (30), we note that all the coefficients have already been determined from Eq. (31) except for the arbitrary constant of integration $A_0^{(5)}$. Adjusting this one free parameter, we find an excellent match of the fit

(black curve) with all of the data (black circles). As was done for the potential, we then predict the energy $U_N(d)$ for other N just by adding or subtracting bulk units

$$U_N(d) = (N-5)U_{\mathrm{b}}(d) + U_5(d). \tag{34}$$

Again, all of the needed bulk coefficients were already determined from Eq. (29) except for the constant term $A_0^{\mathrm{b}} = \Delta U$. The results for $N=2$, 3, and 7 are plotted as the colored curves in Fig. 12. Again, the minima of all the $U_N(d)$ curves match very well the points explicitly calculated in the short-circuit first-principles calculations at various thicknesses. The maximum discrepancy is about 1 meV, which is comparable to the numerical noise in the total energy values introduced by the discreteness of the plane-wave basis set during variable-cell structural relaxations.

Two important details are apparent from Figs. 11 and 12. First, all curves in Fig. 11 have a common intersection at $d=d_0$; this is related to the fact that at $d=d_0$ the internal electric field in the bulk vanishes: $A_1^{\mathrm{b}}=0$ (we shall come back to this point in Sec. III E). Second, the relaxed internal energies of the capacitors considered here are about one order of magnitude larger than the depth of the bulk double well (see Fig. 12). This indicates that the chemical-bonding mechanism discussed in Ref. 7 has a substantial impact on the energetics, which explains the strong tendency of the capacitors toward a superpolar state.

D. Interfacial dielectric and piezoelectric response

Our goal now is to show how several useful interface-specific observables can be directly linked to the *electric* equations of state (EOS) discussed above. In addition to the purely electrical variables, we shall further extend our model by addressing also the *elastic* (i.e., piezoelectric) EOS of both bulk and electrode interface.

1. Dielectric response

The polynomial expansion of the dielectric response (electrical EOS) was essentially already determined in Sec. III C 2. Using the $N=5$ as our model structure and using Eq. (33), we single out the interface contribution by defining the interface EOS to be that of a hypothetical "zero-thickness capacitor"

$$\bar{\varepsilon}_I(d) = \bar{\varepsilon}_0(d) = \bar{\varepsilon}_5(d) - 5\bar{\varepsilon}_{\mathrm{bulk}}(d) \tag{35}$$

with a similar relation for the internal energy. The interface potential and energy are then expanded as in analogy to Eqs. (28)–(31) as

$$U_I(d) = \sum_{n=0}^{3} \frac{A_n^I}{n!}(d-d_0)^n, \tag{36}$$

$$\bar{\varepsilon}_I(d) = \sum_{n=0}^{n} \frac{A_{n+1}^I}{n!}(d-d_0)^n. \tag{37}$$

The coefficients A_n^I are determined once and for all from a pair of calculations on the bulk and on the 5-cell capacitor superlattice using Eq. (32). The resulting bulk and interface coefficients are reported in Table I.

The physical interpretation of the zero-order coefficient A_0^I is immediate as it represents the interfacial contribution to the energy of the capacitor when a reduced displacement d_0 is induced in the film (the energy zero is set to that of the paraelectric $d=0$ state). The first-order coefficient is also physically transparent as it corresponds to the interfacial potential drop at $d=d_0$. As we mentioned above, the bulk ground state at d_0 has zero internal field so an applied external bias of A_1^I will always induce the same (bulklike) polarization, regardless of the thickness N of the film.

In order to interpret the higher-order coefficients, we first derive an expression for the inverse capacitance that is valid for bulk, interface and the full capacitor structure

$$C_{\mathrm{X}}^{-1}(d) = \frac{d\bar{\varepsilon}^{\mathrm{X}}(d)}{dd} = A_2^{\mathrm{X}} + A_3^{\mathrm{X}}(d-d_0), \tag{38}$$

where $X=b,I,(N)$. Therefore, A_2^{X} is the inverse capacitance at $d=d_0$. In the bulk case we can directly link this coefficient[13] to the static (free-stress) dielectric constant of ferroelectric $BaTiO_3$ through Eq. (11)

$$\epsilon_{33}^{(\sigma)} = \frac{4\pi c}{SA_2^{\mathrm{b}}}. \tag{39}$$

Using the values reported in Table I we obtain $\epsilon_{33}^{(\sigma)}=37$.

In the capacitor case the physical meaning of $C_{(N)}^{-1}(d)$ is obvious; note that this is an inverse capacitance per surface unit cell and must be multiplied by S to obtain an inverse capacitance *density*. Finally, $C_I^{-1}(d)$ is the inverse interface capacitance that was discussed, for instance, in Ref. 7. (Note that here C_I is the combined effect of *both* interfaces, unlike the C_I defined in Ref. 7. We shall present a general strategy for separating this quantity into two individual contributions later, in Sec. IV.) By using the values of Table I we obtain an interfacial capacitance density $C_I(d_0)/S=0.44$ F/m^2; this value, due to the dielectric nonlinearity contained in the third-order coefficient A_3^I, is reduced by half near the right end of the d interval considered here ($d\sim 0.55$).

2. Piezoelectric response

In order to describe piezoelectric effects, we consider the bulk lattice parameter c_{b} and the interfacial distance c^I as functions of d. In the same spirit as before, we first perform a quadratic fit of c_{b} as

$$c_{\mathrm{b}}(d) = c_0^{\mathrm{b}} + c_1^{\mathrm{b}}(d-d_0) + \frac{c_2^{\mathrm{b}}}{2}(d-d_0)^2. \tag{40}$$

Here c_0^{b} is the equilibrium lattice parameter of the epitaxially strained tetragonal state and c_1^{b} is related to the piezoelectric constant by Eq. (10)

$$d_{33} = \left.\frac{dc_{\mathrm{b}}}{d\bar{\varepsilon}}\right|_{d=d_0} = \left.\frac{dc_{\mathrm{b}}}{dd}\left(\frac{d\bar{\varepsilon}}{dd}\right)^{-1}\right|_{d=d_0} = \frac{c_1^{\mathrm{b}}}{A_2^{\mathrm{b}}}. \tag{41}$$

With the calculated values, we obtain $d_{33}=30$ pm/V. (Note that in our calculations we kept the in-plane lattice param-

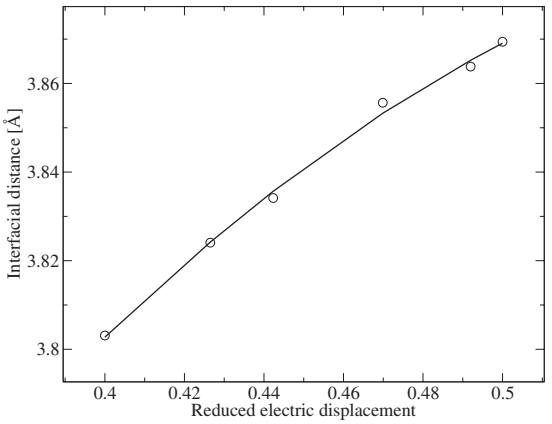

FIG. 13. Calculated interfacial distance $c^I(d)$ of Eq. (42) for capacitors of various thicknesses and polarization states (symbols); solid curve is a quadratic fit.

eters fixed; this value might change upon full relaxation of the crystal.)

Next, we define the interface contribution $c^I(d)$ as

$$c^I(d) = L_N(d) - Nc_{\text{bulk}}(d) - n_{\text{Pt}}\delta_{\text{Pt}}. \tag{42}$$

where $L_N(d)$ is the total thickness of the relaxed capacitor for a given value of d, and N and n_{Pt} are the number of oxide and metal bulk cells in the capacitor superlattice. Note that δ_{Pt}, the relaxed interlayer distance in bulk Pt (strained in plane to the same lattice parameter), is independent of d. Using this formula, we extracted $c^I(d)$ for all the capacitor structures considered so far and plotted the values in Fig. 13. In the same figure the solid line is a quadratic fit using the formula

$$c^I(d) = c_0^I + c_1^I(d - d_0) + \frac{c_2^I}{2}(d - d_0)^2. \tag{43}$$

The zeroth-order coefficient c_0^I has the meaning of a combined effective interface distance for both top and bottom electrodes. (It may look larger than expected because there are actually $N+1/2$ oxide cells in our capacitors, not N, and because the Pt/BTO interface distances are typically somewhat larger than the bulk interlayer spacings of either Pt or BTO.) The linear coefficient, in analogy to the bulk case, is related to the electrode contribution to the piezoresponse of the capacitor. All the coefficients defined in the text are reported in Table I.

In summary, our simple model is able to predict, within the numerical accuracy of a *full* first-principles calculation, the energy, polarization, dielectric, and piezoelectric response of a Pt/BTO/Pt capacitor of arbitrary thickness (from 2 unit cells to infinity).

E. Band lineup and ferroelectricity

The simple model derived above allows us to interpret the physics behind the polar enhancement from yet another point of view. If we go back to Fig. 11, it is apparent that the solid lines converge to the same point at a value of d corresponding to the spontaneous polarization of bulk $BaTiO_3$ ($d_0 = 0.364$). The reason is that the potential is zero in $BaTiO_3$ at that value of d because the bulk crystal is at electrostatic equilibrium; hence, adding or subtracting bulk units does not change the value of $\bar{\varepsilon}_N(d_0)$. Therefore, $\bar{\varepsilon}_I(d_0) = \bar{\varepsilon}_N(d_0)$, independent of N, is an intrinsic interface property related to the band lineup between the metal electrode and the fully polarized ferroelectric film

$$\bar{\varepsilon}_I(d_0) = A_1^I = \phi^+ - \phi^-, \tag{44}$$

where $\phi^\pm$ are the respective Schottky barrier heights at the positively and negatively polarized ends of the film. Since the symmetry is broken on ferroelectric off centering, these two values generally differ.

Based on typical assumptions of phenomenological theories and on a large body of experimental data, one would expect a positive interface potential $\bar{\varepsilon}_I(d_0) > 0$; in short circuit this would yield a depolarizing field that *opposes* the polarity of the film (recall that $\bar{\varepsilon} = -V$). This means that generally one needs to apply a positive bias in order to reach (and sustain) bulk values of d in a thin film; when the bias is switched off, the polarization is either reduced or relaxes to zero by transitioning to a multidomain state.[32] The Pt/BTO/Pt system analyzed in this work displays a rather different behavior, in that $\bar{\varepsilon}_I(d_0) \sim -0.8$ V is *negative*. This is a signature of the strong *polarizing* field discussed earlier in the context of our calculations in short circuit.

Note that in our calculations so far we never extracted ϕ^+ and ϕ^- separately since in the case of compositionally symmetric capacitors only their difference matters for the electrical properties of the device. Analogously, we considered only a *total* interfacial distance c_I that takes into account both the top and bottom ends of the film. In the following sections we shall use the techniques described in Sec. II D 2 to single out the potential lineup and distances of either interface individually as a function of d. We shall demonstrate, as an example, how this information allows one to accurately model the electrical behavior of truly asymmetric devices starting from calculations performed on systems having a centrosymmetric paraelectric geometry.

IV. RESULTS: Au/$BaZrO_3$/Au CAPACITORS

A. Motivation

As a model system for studying the electrical behavior of asymmetric capacitors we choose ferroelectric devices with Au as the electrode and $BaZrO_3$ (BZO) as the active film. This choice is motivated by issues of computational practicality. As mentioned in the introductory sections, an essential prerequisite for defining and controlling the polarization in a metal/insulator heterostructure is its insulating character along the direction perpendicular to the interface. This can only be true if there are nonvanishing Schottky barriers at both interfaces and if those barriers are preserved on ferroelectric off centering. The wider band gap of BZO makes this property much easier to satisfy than with more conventional ferroelectric oxides such as $PbTiO_3$ and $BaTiO_3$. Then, given the larger lattice parameter of BZO, we decided to use Au as the electrode instead of Pt in order to avoid unrealistically

large strains in the electrode slab. (Pt is more popular in the ferroelectrics community because it matches better the lattice parameter of many Ti-based perovskites.) This combination of materials yields large Schottky barriers for both BO_2- and AO-terminated interfaces and is therefore ideally suited to the scope of the present study. An interesting aspect of this study is that we are able to compare the electrical behavior of BO_2- and AO-terminated interfaces.

One important issue is that BZO is not ferroelectric. Experimentally it has a stable cubic structure down to very low temperatures while theoretically there have been several reports of zone-boundary instabilities associated with rotations of the oxygen octahedral.[33] In order to induce a polar instability in BZO, we set the in-plane lattice parameter to a fixed value of 7.60 a.u. (a compressive strain of −3.0% with respect to the theoretical equilibrium lattice parameter of 7.38 a.u. of the cubic structure).[34] Note that we did not check for possible competing nonpolar states as such an analysis would require doubling the size of the simulation cell, substantially raising the computational cost. For this reason, our setup should not be understood as a direct prediction of ferroelectric behavior in epitaxially strained $BaZrO_3$. Rather, we intend it primarily as a tractable computational model, which we expect may be representative of the behavior of a typical perovskite with a tetragonal ferroelectric ground state (e.g., $PbTiO_3$ or $BaTiO_3$ at room temperature).

B. Computational model

Our model heterostructures consist of (001)-oriented BZO films with symmetrical ZrO_2 or BaO terminations and a thickness of 8.5 unit cells, interfaced with a metal electrode slab of 11 Au monolayers. Our first goal is to study the full equations of state of these structurally *symmetric* capacitors to establish the similarities and the differences arising from the dissimilar (ZrO_2/Au vs BaO/Au) bonding configurations. Next we extract the interface-specific information and use it to predict the full equation of state of an *asymmetric* configuration (with BaO and ZrO_2 terminations at opposite ends). Then, we verify that our procedure yields the desired result by comparing this prediction with the explicitly computed $U(d)$ curve for an asymmetric capacitor having 8-unit cells of BZO and 12 layers of Au. Before going into details about the capacitor structures, however, we first briefly summarize the electrical properties of bulk $BaZrO_3$ within the symmetry and mechanical constraints described above.

C. Bulk $BaZrO_3$

As in the capacitor structures, we fix the in-plane lattice constant to $a_0=7.60$ a.u. and let the out-of-plane lattice parameter as well as the internal coordinates of the five-atom tetragonal unit cell, relax as a function of the reduced electric displacement d. We use seven evenly spaced values of d ranging between $d=0.0$ and $d=0.276e$. We extract from the calculation the values of the reduced field $\bar{\varepsilon}$ and the lattice parameter c for each value of d, use splines to interpolate these values, and finally integrate $\bar{\varepsilon}(d)$ with respect to d to recover the internal energy $U(d)$. The results are reported in Fig. 14. As for the $BaTiO_3$ case, the match between the values of U calculated directly (red "plus" symbols) with those obtained by integrating $\bar{\varepsilon}(d)$ (black curve) is excellent. Both the spontaneous polarization P_s and the double-well potential depth ΔU are significantly smaller than in $BaTiO_3$. The relaxed ferroelectric ground state is at $d=0.2076$, which corresponds to $P=20.5\ \mu C/cm^2$, $\Delta U=-3.05$ meV/cell, and $c/a=1.052$ (compared to $c/a=1.0475$ in the strained centrosymmetric geometry).

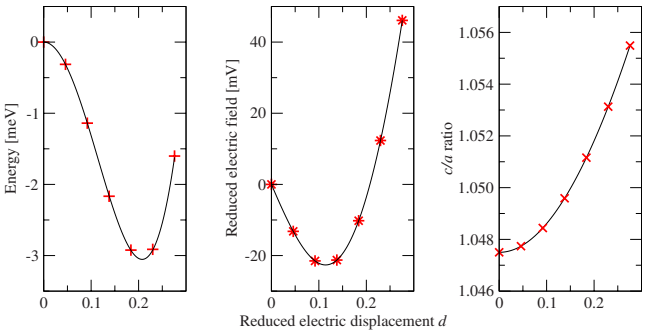

FIG. 14. (Color online) Internal energy, reduced electric field, and c/a ratio vs reduced displacement field (in units of e) for coherently strained bulk $BaZrO_3$. *Ab initio* data are shown as symbols; dashed curves in the middle and right panels are spline interpolations; and continuous curve in the left panel is the numerical integral of the spline in the middle panel.

D. Schottky barriers

In Fig. 15 we plot, as a function of the reduced displacement d, the SBH extracted from the symmetric BaO- and ZrO_2-terminated capacitors using the techniques of Sec. II D 2. All values lie between about −1.2 and −1.7 eV. Considering that the calculated local-density approximation gap for centrosymmetric bulk $BaZrO_3$ is 3.12 eV, this indicates that in all cases the Fermi level of Au lies close to midgap and that our BZO/Au capacitors are thus free from Schottky-

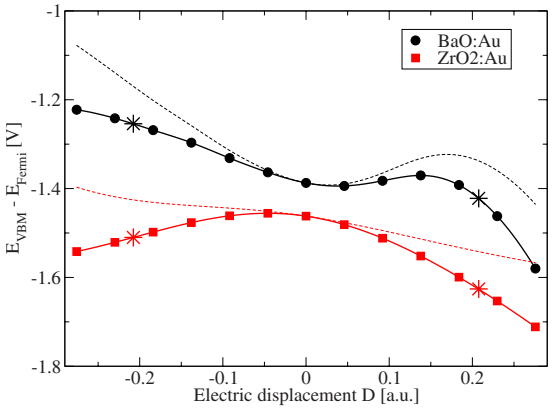

FIG. 15. (Color online) Solid curves: interfacial p-type Schottky barrier values extracted from the symmetric capacitor configurations for BaO-terminated (black circles) and ZrO-terminated (red squares) films. Dashed curves: same, except that the bulk dependence of the VBM on the electric displacement has been subtracted out. The sign of d follows the convention that the electrode lies at $z>0$.

breakdown issues.[4] Both curves shown in Fig. 15 have considerable curvature although with dissimilar features. In the case of ZrO_2/Au this curvature is found to be dominated by the bulk $\Delta V_F(d)$: If we remove such a dependence from $\phi_{ZrO}(d)$, we obtain a roughly linear function (red dashed curve, which is related modulo a constant shift to the interfacial step in the electrostatic potential). By contrast, removal of the bulk contribution $\Delta V_F(d)$ (black dashed curve) does not restore linearity in the BaO/Au case.

Incidentally, we note that our method may be of general use for the computation of Schottky barriers[35,36] (independently from their relationship to dielectric properties), which are extremely important for many technological applications. Recall that the SBH has a truly unique definition only when the macroscopic electric field vanishes in the insulator since then one can identify the valence- and conduction-band edges precisely. For noncentrosymmetric insulators such as wurtzite oxides or spontaneously polarized ferroelectrics, such a condition is not easily obtained in ordinary first-principles supercell calculations. However, our approach makes it extremely easy to do such calculations. For example, we have indicated with large "star" symbols in Fig. 15 the "physical" values of the SBH, i.e., those corresponding to the spontaneously polarized ferroelectric film in the absence of any internal field.

E. Interfacial equation of state: ZrO_2/Au

The discussion in the previous section suggests that there might be important qualitative differences between the behavior of BaO/Au and ZrO_2/Au interfaces. However, it is not immediately obvious how to interpret the $\phi(d)$ curves directly as their relationship to the physical electrical response of the capacitor contains some aspects of arbitrariness. Such arbitrariness does, of course, cancel out when the final equation of state of the entire capacitor is constructed. Therefore, in order to obtain quantities that have a direct physical meaning, we proceed by combining the above $\phi(d)$ curves in pairs as appropriate for the capacitor structures of interest. There are four such structures that we denote as "*AB*," where *A* and *B* are variables that specify, for the bottom and top interfaces respectively, whether the interface is BaO/Au or ZrO_2/Au. Then the interface contribution to the equation of state of the specified capacitor structure is

$$\bar{\varepsilon}_{I,\mathrm{AB}}(d) = -\phi_{\mathrm{A}}(-d) + \phi_{\mathrm{B}}(d) \tag{45}$$

in terms of which the equation of state of the entire *N*-cell capacitor is then $\bar{\varepsilon}_{N,\mathrm{AB}}(d) = \bar{\varepsilon}_{I,\mathrm{AB}}(d) + N\bar{\varepsilon}_{\mathrm{b}}(d)$.

The four resulting functions $\bar{\varepsilon}_{I,\mathrm{AB}}(d)$ are plotted in Fig. 16. The most striking feature is the almost perfect linearity of the symmetric ZrO_2/ZrO_2 configuration. This means that the description of the interfacial equation of state in terms of a constant interfacial capacitance (i.e., replacing the interfaces by a layer of linear dielectric in series with a bulklike $BaZrO_3$ film) is appropriate in this case. The slope of the $\bar{\varepsilon}_I(d)$ curve yields a combined capacitance density of $C_I/S = 1.73$ F/m^2 for both interfaces so that each interface is associated with a capacitance density of 3.46 F/m^2. This value is remarkably high when compared to the typical range of

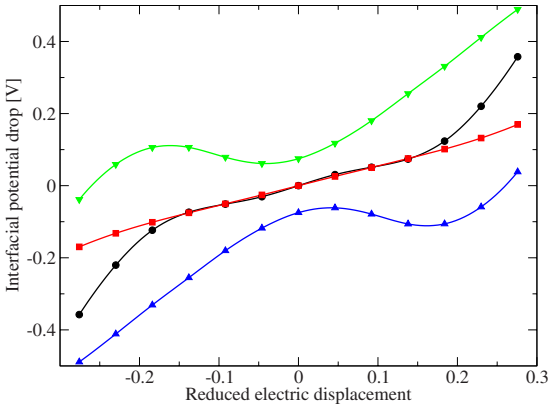

FIG. 16. (Color online) Interfacial equations of state, reconstructed from the Schottky barrier values of Fig. 15, for a symmetric BaO-(black circles) or ZrO_2-terminated (red squares) capacitor. The blue upward-oriented triangles refer to an asymmetric arrangement with the BaO termination on top; the green downward-oriented triangles have the BaO termination at the bottom.

$\sim 0.4-0.6$ F/m^2 calculated[7,37] for oxide electrodes such as $SrRuO_3$. This result corroborates the ideas proposed in Ref. 7 that weak electrode-oxide bonding is beneficial to the ferroelectric properties of a capacitor. Here we indeed find that a chemically inert electrode material such as Au yields excellent screening and only a marginal perturbation to the polar response of the film. Using the formalism developed in Ref. 7, we find a "critical thickness for ferroelectricity" $N_{\mathrm{crit}}=3$ for both symmetric geometries (ZrO_2/ZrO_2 and BaO/BaO).

F. BaO/Au and bonding properties

Interestingly, the BaO/BaO curve is almost exactly overlapping with the ZrO_2/ZrO_2 one in the interval $-0.15e < d < 0.15e$ while a strong departure from the linear regime occurs for values of *d* lying outside this interval. A significant nonlinearity was indeed expected from the $\phi(d)$ curves in Fig. 15; the fact that this nonlinearity cancels for $-0.15e < d < 0.15e$ and yields a quasilinear behavior is probably coincidental.

The nonlinearity of the BaO/Au interface emerges most clearly in the case of an asymmetric capacitor (green and blue curves in Fig. 16, which are correctly related by a mirror-symmetry operation).

To trace the origin of the qualitative difference between ZrO_2/Au and BaO/Au interfaces (linear vs nonlinear behavior), it is useful to follow the evolution of the Au-O bond length as a function of electric displacement, plotted in Fig. 17. While the bond length varies only weakly and follows a linear trend for ZrO_2/Au, it covers a much wider range of distances (2.2 to 3.1 Å) and displays a strong nonlinearity for BaO/Au. We interpret the latter behavior as indicative of breaking and reforming of the Au-O bond upon polarity switching. Clearly, the breaking of a bond is a highly nonlinear event, helping to explain the calculated features of the electrical response. This picture agrees fully with the arguments of Ref. 7, where the bond stability (instability) was correlated with the suppression (enhancement) of the ten-

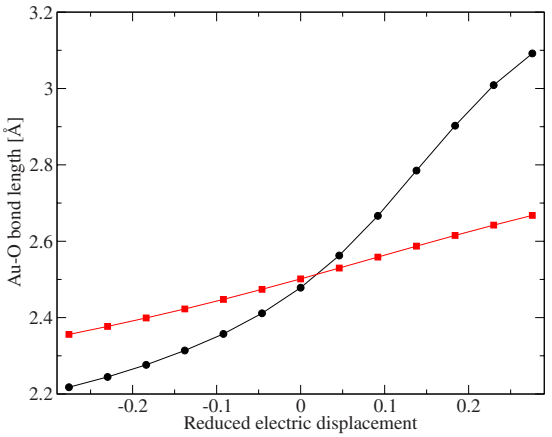

FIG. 17. (Color online) Interfacial Au-O bond distance as a function of electric-displacement field. The sign of d follows the convention that the electrode lies at $z>0$.

dency to polar instability of the capacitor structure. The present results corroborate these ideas and provide further evidence for the strong correlation between interfacial chemistry and electrical response.

Interestingly, while in the case of $Pt/BaTiO_3/Pt$ the interface bonding mechanism strongly enhances ferroelectricity, in the present case of $Au/BaZrO_3/Au$ the overall effect is a slight suppression. We shall briefly discuss the origin of this dissimilar behavior in the following section.

G. Enhancement or suppression?

Why do certain AO-terminated interfaces (e.g., $BaTiO_3/Pt$ and $BaTiO_3/Au$) enhance the ferroelectric instability of the film while others (especially $PbTiO_3/Pt$ but also, to a smaller extent, the $BaZrO_3/Au$ one discussed here) suppress it instead? While a definitive answer is not yet available, some qualitative trends can be explained in terms of the frustrated bonding-environment model of Ref. 7. According to this model, a flat layer in contact with the electrode produces a competition between the A-metal repulsion and the -metal attraction. The buckling of the AO layer caused by a bulk ferroelectric distortion of one sign or the other shifts the balance, causing the bonding or the repulsive force to prevail. In fact, even in the centrosymmetric capacitor geometry, the interface AO layer is not flat but exhibits a certain degree of buckling (with the A cation typically displacing toward the oxide film) due to the broken-symmetry environment. One can therefore expect some difference in behavior between perovskite AO-terminated films that show different degrees of "natural buckling" at the surface of their cubic reference phase. We computed the values of the AO rumpling of the free $PbTiO_3$, $BaZrO_3$, and $BaTiO_3$ surfaces, finding values of 0.136, 0.121, and 0.022 Å, respectively. Indeed, these results indicate that the film with the much flatter surface ($BaTiO_3$) displays a strong enhancement of the polar instability while those that are significantly buckled ($PbTiO_3$ and $BaZrO_3$) do not. While this is only a rough indication and other factors are most likely at work, it suggests a correlation that may help to explain our detailed numerical results.

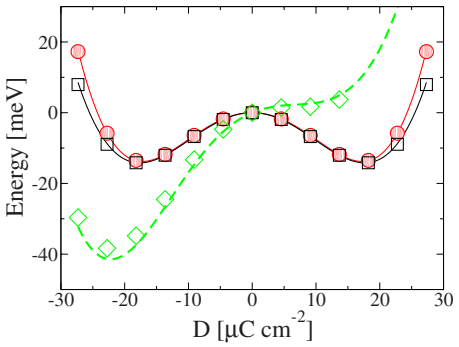

FIG. 18. (Color online) Electric equation of state $U(D)$ for three capacitor configurations discussed in the text. Curves correspond to integrating Eq. (19) [or Eq. (46)], where $\phi_{L,R}(d)$ were extracted from the symmetric capacitor calculations (solid curves in Fig. 15) and $\bar{\varepsilon}_{bulk}(d)$ was extracted from the bulk calculation (middle panel of Fig. 14). Points correspond to the $U(d)$ values explicitly calculated for symmetric BaO:BaO (black squares), symmetric ZrO_2:ZrO_2 (red circles), and asymmetric BaO:ZrO_2 (green diamonds) capacitors.

H. From symmetric to asymmetric

We claimed earlier that it should be possible to use the interface equations of state extracted from calculations on *symmetric* capacitors to predict the equation of state for the *asymmetric* case. We demonstrate this now. Our "asymmetric" geometry is comprised of an 8-unit-cell $BaZrO_3$ film and a 12-layer Au slab, where the bottom and top interfaces (relative to the oxide) are of Au-BaO and ZrO_2-Au type, respectively. Thus, a positive d corresponds to the polarization pointing toward the ZrO_2-Au interface. The interface-specific contribution to the reduced electric field, $\bar{\varepsilon}_I(d)=-\phi_L(d)+\phi_R(d)$, is plotted as the green curve in Fig. 16. Note that the curve is linear for $d>0$ while it shows a significant nonlinearity for $d<0$, where the Au-O bond breaks, in agreement with the discussion of the previous sections. We now use this function to reconstruct the $\bar{\varepsilon}(d)$ curve of the whole capacitor by adding an appropriate number of bulk units as in Eq. (19)

$$\bar{\varepsilon}(d) = \bar{\varepsilon}_I(d) + N\bar{\varepsilon}_{bulk}(d) \tag{46}$$

with $N=7.5$.[38] Then we numerically integrate $\bar{\varepsilon}(d)$ to obtain the $U(d)$ energy curve, which is plotted as the dashed green curve in Fig. 18.

In the same figure we plot two other curves corresponding to the symmetric geometries, which were obtained from the symmetric curves in Fig. 16 in the corresponding way (with $N=8$). For all three curves we also plot, as symbols, the values of U extracted directly from the first-principles calculations. The match is almost perfect for the symmetric cases as expected since the potentials and energies were taken from the *same* calculation; their agreement is just a test of internal consistency. (Incidentally, note the close agreement between red and black curves in Fig. 18, especially in the central region, which is inherited from the similarity of the corresponding red and black curves in Fig. 16.) The acid test, however, concerns the asymmetric structure: the points were extracted from a direct calculation on the asymmetric structure while the curve was inferred from the data on symmetric

capacitors using our model of Eq. (19). The match is excellent, with less than a 1% discrepancy in the spontaneous polarization at the minimum in Fig. 18, corresponding to short-circuit boundary conditions. (The predicted and calculated D values are −22.1 and −22.2 $\mu C/cm^2$, respectively.) Note that the spontaneous D is significantly enhanced (~8%) compared to the bulk value. This is a consequence of the nonlinearity discussed above, which induces a *positive* $\bar{\varepsilon}_I$ for $d<0$ (see green curve in Fig. 16). The prediction and the actual calculation also nicely agree regarding the absence of a secondary minimum at positive d. Interestingly, both strategies would yield such a minimum if the capacitor were just one unit cell thicker; this further confirms the accuracy of our model.

While all these physical aspects compare very favorably, Fig. 18 shows also some discrepancies in the actual values of the internal energy U, in particular, concerning the depth of the energy minimum (predicted and calculated ΔU values of −38.4 and −41.4 meV, respectively). We shall briefly discuss this discrepancy in the following Section.

I. Accuracy issues

We demonstrated in Sec. III that the locality principle established in Sec. II holds very accurately, allowing one to predict the electrical properties and energetics of capacitors of varying thickness with excellent fidelity. In this respect the discrepancy in the energy curves of Fig. 18 is somewhat surprising and it is worth discussing its origin to make sure that all aspects of the method are under control.

We find that the cause of the discrepancy is rooted in the treatment of the Au electrode in the simulations rather than in numerical (or formal) errors. In the symmetric calculation, we used an 11-layer Au slab and from this data we constructed the green curve in Fig. 18. On the other hand, we had to choose an even (12-layer) Au slab in the asymmetric calculation, which yielded the green diamond symbols. It is well known that quantum-size effects associated with Fermi-surface nesting can persist to substantial thicknesses in thin metal films.[39] Thus, it is not unreasonable to expect the surface of a 12-layer slab to behave slightly differently from that of an 11-layer slab. To prove this point, we calculated the work function of two free-standing slabs of 11 and 12 layers, and we found a difference of about 60 meV—enough to produce non-negligible discrepancies in the capacitor calculations. The use of a finite electronic temperature (to accelerate convergence with respect to k-point sampling) helps, in that it makes the one-particle density matrix of the metal short-ranged in space. However, further exploration of these issues falls outside the main scope of the present work and we satisfy ourselves with advising the reader of this issue so that it can be kept in mind when performing future calculations.

V. DISCUSSION

In the following, we discuss the implications of our work by comparing our techniques and results to the relevant literature.

A. Locality

One of the crucial aspects of our work concerns the use of the locality principle in the simulation of capacitor structures. As we mentioned in the introduction, at least two recent theoretical works have reported phenomena which do not appear consistent with this assumption. We shall briefly discuss them here.

First, the authors of Ref. 11 reported, for BaO-terminated $Pt/BaTiO_3/Pt$ capacitors (structurally analogous to those considered in Sec. III), a "ferrielectric" LP pattern, with profound qualitative deviations from the bulk pattern, affecting the whole volume of the oxide film. This, in principle, implies a sharp, qualitative, deviation from the locality principle mentioned above. While we cannot provide a definitive explanation for the origin of the disagreement with our results, we believe it might lie in the subtleties involved in the LP construction for an overall metallic system such as the ferroelectric capacitors under consideration. In contrast with our work, where localization of the Wannier states is imposed in one dimension separately for each k point (as in the original LP formulation in Ref. 19), the authors of Ref. 11 used fully three-dimensional maximally localized Wannier functions. Furthermore, they treated the metallic states rather differently than here, in that they adopted a preliminary disentanglement[40] procedure before localizing the states by means of the Marzari-Vanderbilt algorithm.[17] Finally, the authors of Ref. 11 might have taken different prescriptions for the assignment of the Wannier functions to the individual oxide layers, possibly introducing the LP equivalent of the quantum of polarization in their reported values. Regardless of which of the above factors may be responsible for the discrepancy, the effect proposed in Ref. 11 appears likely to be a consequence of the details of the Wannier localization/grouping procedure and we therefore suggest that its physical significance should be judged with some caution.

Second, the authors of Ref. 10 considered $SrRuO_3/KNbO_3/SrRuO_3$ capacitors and reported an interface-induced disruption of the ferroelectric soft mode of the film with the appearance of a head-to-head "interface domain wall" located 3 unit cells away from the electrode. This was interpreted as an effect of the strong bonding at the interface, which would "clamp" the interface dipoles to a fixed value; this constraint would then couple with the ferroelectric instability of the film, producing the calculated inhomogeneous polarization pattern. The spatial variation in P is strongly asymmetric and takes place over approximately 6 unit cells at the positively polarized end of the $KNbO_3$ film.[10] This contrasts with our results, where the interface-induced distortions are extremely local and heal completely within the first perovskite unit cell adjacent to the interface. Even if the metal-insulator interactions are somehow stronger for the $SrRuO_3/KNbO_3$ system than for our cases, this should just be reflected in a stronger functional dependence in the interface equation of state, modifying the strength of the depolarizing field. One should still expect a uniform polarization deep in the insulator, unlike the inhomogeneous polar ground state found by these authors. Therefore, it is difficult to understand their findings unless one of the fundamental prerequisites for the formalism developed in this work might have

broken down. For example, Junquera and Ghosez[4] have emphasized the dangers of pathological band alignments which, as an artifact of the band-gap problem of density-functional theory, may lead to charge spillage into the perovskite at certain perovskite-metal interfaces. We suggest that such a possibility should be investigated for the $SrRuO_3/KNbO_3$ interfaces considered in Ref. 10.

B. Relationship to Landau theory

Our approach has many points of contact with earlier Landau-theory models of depolarization in thin-film ferroelectrics. However, there are also some notable differences that we shall emphasize in the following, in order to avoid confusion or misunderstanding.

First, we note that our strategy is different in spirit from what was done, for example, in Ref. 41. There, the authors fitted the parameters of a Landau-type expansion to the calculated first-principles values of the depolarizing field in short-circuited capacitors. In contrast, in our approach the first-principles engine works as a stand-alone tool that yields the ground state energy and structure as a function of a well-defined electrical variable (within a given set of specified mechanical/symmetry constraints and thermodynamic ensemble). These data can then be fitted *a posteriori* to a polynomial, thus obtaining an expression that bears a close resemblance to Landau-theory expansions but the latter is not a necessary step.

Another difference concerns our use of an interfacial capacitance (or, equivalently, of an effective screening length) that embodies all the physical ingredients contributing to the electrostatics. Gerra and co-worker,[42] on the contrary, made a distinction between purely electrostatic screening and short-range chemical bonding effects, and considered them separately in the capacitor equation of state. While such a distinction appears desirable from a conceptual point of view, implementing it in practice involves a kind of chicken-and-egg problem. As we have shown in Ref. 7, screening and interface bonding are strongly interrelated and it is not obvious how to distinguish cause and effect. At first sight, our approach does not appear to provide a solution to the above dilemma as we cast "everything" (chemical bonding and short- and long-range Coulomb interactions) into a black box, namely, the interface equation of state. However, on closer inspection our method does implicitly provide such a separation. In fact, by explicitly working as a function of a controlled field (here the D field), we automatically ensure that only the ingredients that are electrical in nature are included in the interface equations of state, $V_I(d)$. The nonpolar contributions, which are short-ranged and do not have any direct impact on the electrostatics, merely enter the definition of the zero of the energy, and are therefore implicitly (but rigorously) singled out.

Finally, we would like to comment briefly on our choice of D as electrical variable; such a choice is rather convenient, as we have shown in this work. Interestingly, using D is frowned upon by some authors in the Landau-theory community,[6,14] especially in cases where depolarizing effects are present. A detailed discussion of this issue would bring us far from the main scope of our work. We limit ourselves to noting that, by means of our fixed-D approach, we seek the electronic and structural ground state at a given D within a parameter space spanned by all the *microscopic* degrees of freedom (which are implicitly present in our energy functional). This means that our description fully accounts for the effects of the "background permittivity," of hypothetical competing instabilities, and of electromechanical couplings. For this reason, it is free from the shortcomings described in Ref. 14. An important point to stress is that, *in well-behaved cases*, the electrical equation of state of a given system leads to exactly the same description of the physics regardless of which independent variable (electric field $\mathcal{E}$, polarization P, or electric displacement D) is used. This point is obvious in linear dielectrics, where $P=\chi\mathcal{E}$ and $D=\epsilon\mathcal{E}$. It still holds in nonlinear dielectrics that have a single energy minimum as a function of the applied field $\mathcal{E}$. In more problematic cases, the equation of state might become multivalued or even singular, depending on the choice of independent variable. In our experience, D tends to be a very convenient choice, especially in these "difficult" situations.

C. Relationship to the effective-Hamiltonian approach

One of the strengths of our approach is the ability to recast all the complexity of the interface interactions into a smooth function of a single electrical variable. This naturally leads to powerful modeling strategies as we demonstrated in practice in Secs. III and IV. An obvious next step would be to combine the interface information derived from first principles with higher-level "effective Hamiltonian" descriptions of the ferroelectric film,[43,44] in order to describe phenomena that involve larger length and/or time scales (e.g., ferroelectric switching).

Effective-Hamiltonian approaches have been used quite intensely in the past few years to investigate size effects in ferroelectric nanostructures[45–48] such as films, wires, and dots. Generally, the effective Hamiltonian is formulated and fitted in order to describe *bulk* behavior, as follows. One first identifies a reduced set of local-mode variables to describe the amplitudes of the soft ferroelectric mode and strains within each unit cell. Then a model of the energy, written as an expansion in these local-mode degrees of freedom, is constructed, and the parameters in the expansion are fitted to a database of first-principles calculations. Among the parameters determined in this way are some that correspond to short- and long-range dipolar interactions. The finite-temperature statistical behavior of the system can then be simulated using Monte Carlo or molecular-dynamics techniques.

In order to simulate a nanostructure, the effective Hamiltonian description is typically applied without modification to a 2D, 1D, or zero-dimensional (0D) system. This approach has allowed for important conceptual advances, for instance, by elucidating the properties of polarization vortices in nanodisks and nanorods;[47] in such configurations the lower dimensionality is largely responsible for the peculiar behavior. However, in the case of 2D systems such as ferroelectric superlattices or thin-film capacitors, an important conclusion

of our work is that the fine details of the interface bonding and electrostatics are crucial to determining the overall physical behavior of the system. In that sense, the simple abrupt truncation of the dipolar interactions[30] which is assumed in the H_{eff} simulations discussed above may fall short of faithfully reproducing the overall response of a realistic device.[7] Including the interface-specific information in a thin-film effective-Hamiltonian model would therefore be very desirable.

For example, for a given interface, one could evaluate the interface EOS of the H_{eff} at zero temperature ($T=0$) and compare with the one computed *ab initio* using the methods described in this work. One could then modify the parameters of the H_{eff} in the vicinity of the interface until the $T=0$ interface EOS agrees with the first-principles one. This would then enable one to answer important questions that cannot be directly addressed from first principles. For example, what is the temperature dependence of the interface equation of state? Or, what is the impact of the electrode on the stability of the monodomain state versus a polydomain one? Finally, by making use of the locality principle discussed in this work, it would be relatively easy to analyze the H_{eff} results and compare them to the fully first-principles values with significant benefit for both theories. To substantiate these arguments, in the following we shall briefly discuss two selected H_{eff} works that are particularly relevant in light of our proposed strategy.

In Ref. 48, Bin-Omram *et al.* investigate the impact of electrical and mechanical boundary conditions on the polarization and strain of $BaTiO_3$ and $Pb(Zr,Ti)O_3$ (PZT) films. For a $BaTiO_3$ film at a 2.0% compressive strain, which roughly corresponds to the $SrTiO_3$ substrate assumed in our calculations, the authors of Ref. 48 find a spontaneous polarization that increases for thinner films with a value of 0.56 $\mathrm{C/m^2}$ at a thickness of 6 unit cells. This is qualitatively similar to the effects we discussed in Sec. III for $Pt/BaTiO_3/Pt$ capacitors although significantly larger in magnitude. We stress that such an enhancement is far from being a systematic property of electroded $BaTiO_3$ films;[7] as we suggested above, the surface terms in H_{eff} should be adapted to the specific electrode interface on a case-by-case basis.

In Ref. 49 the authors report that 2D, 1D, and 0D ferroelectric nanostructures are characterized by "dielectric anomalies" in the form of a negative internal susceptibility $\chi^{(\mathrm{int})}$. It is not unreasonable to think that the surface-induced enhancement of the ferroelectric instability, which is built into most H_{eff} thin-film models, may be largely responsible for the reported negative $\chi^{(\mathrm{int})}$ in the 2D case. Note that $\chi^{(\mathrm{int})}$ is defined there as an average over the volume of the film, unlike our definition of the local dielectric permittivity $\epsilon(x)$,[50] which was introduced in Refs. 16 and 20. This further highlights the conceptual advantage of rigorously separating bulk and surface/interface effects by performing a *local* analysis rather than global averages. Overall, we believe that the methods developed in this work open interesting avenues for the accurate simulation of ferroelectric nanostructures within the H_{eff} framework.

D. Interpretation of experimental data

In this section, we ask how one might best make contact between an experimental set of electrical measurements on a series of thin-film capacitors of varying thickness on the one hand and the analysis tools we developed in Secs. III and IV on the other. Of course, it is best if the experiment can approach intrinsic conditions insofar as possible. For example, the experimental film should ideally be in a monodomain state. This may be hard to achieve in short circuit, as depolarizing effects might induce a multidomain state[6,51] but often may be obtained by applying a dc bias to the capacitor as in Ref. 32. Also, the film should be as free as possible from space charges arising from charged defects or trapped carriers, which may contribute to band-bending effects not considered in the theory.

Our first prediction is that there exists a value of the external bias, A_1^I that yields the same value d_0 of the spontaneous electric displacement regardless of the film thickness (provided that the interfaces and the film quality are similar). Our second prediction is that, around this bias value, the inverse capacitance of the films should scale linearly with thickness with the coefficient of proportionality being directly related to the bulk permittivity. Assuming a small range of biases around A_1^I, we can discard the third-order coefficients A_3 and write

$$\bar{\varepsilon}_N(d) = A_1^I + (d - d_0)A_2^{(N)} \tag{47}$$

with

$$A_2^{(N)} = A_2^I + NA_2^{\mathrm{b}}. \tag{48}$$

We end up with three coefficients that describe the electrical properties of the capacitors and their dependence on thickness.

To obtain this information, we believe it is best to represent the data in a $(P,\bar{\varepsilon})$ plot as in Fig. 11 rather than a $(P,\mathcal{E})$ plot as is usually done (note that $\bar{\varepsilon}$ corresponds to minus the applied bias potential V). In this way, one obtains direct visual insight into the existence of a common intersection point (P_0,A_1^I). Note that the bulk A_2^{b} coefficient provides, as a byproduct, useful information on the dielectric properties of the film through Eq. (39), as it is independent of the specific interface. (In principle, it depends only on the applied strain due to epitaxial matching and of course on the operating temperature.) By combining Eqs. (47) and (48) we obtain, for the spontaneous polarization of a short-circuited capacitor of a given thickness N

$$P_0^{(N)} \sim P_0^{(b)} - \left(\frac{4\pi}{S}\right)\frac{A_1^I}{A_2^I + NA_2^{\mathrm{b}}}. \tag{49}$$

Note that, in typical phenomenological models, the interface is treated as a linear dielectric, which implies $A_1^I = d_0 A_2^I$. A_2^I is related to the interface capacitance C_I and to the effective screening length λ_{eff} by

$$\frac{1}{2}A_2^I = C_I^{-1} = \frac{4\pi}{S}\lambda_{\text{eff}}. \quad (50)$$

The factor of one-half on the left-hand side relates to the assumption of two equivalent interfaces with identical electrical properties.

VI. CONCLUSIONS

We have developed a comprehensive methodological framework for the computation and analysis of ferroelectric capacitors with realistic electrodes. Our method is based on density-functional theory and on recently-developed techniques for performing calculations at a given value of the electric-displacement field. By making a rigorous separation between the interface and bulk contributions to the electrical equation of state of a capacitor, we obtain a compact model, of full first-principles accuracy, for the electrical (and piezoelectric) response as a function of bias potential and thickness. We expect these advances to facilitate the comparison of theory with experimental data. We also hope that it will stimulate a fruitful interaction with other theoretical approaches based, e.g., on Landau theory or effective Hamiltonians. Application of similar strategies to investigating the interface coupling between electric polarization, magnetism, and other structural degrees of freedom (such as octahedral tilting) that were not considered here are under way.

ACKNOWLEDGMENTS

This work was supported by the Department of Energy, SciDac program on Quantum Simulations of Materials and Nanostructures under Grant No. DE-FC02-06ER25794 (N.A.S. and M.S.) and by ONR under Grant No. N00014-05-1-0054 (D.V.).

[1] J. F. Scott, Science **315**, 954 (2007).
[2] M. Dawber, K. M. Rabe, and J. F. Scott, Rev. Mod. Phys. **77**, 1083 (2005).
[3] K. M. Rabe, Curr. Opin. Solid State Mater. Sci. **9**, 122 (2005).
[4] J. Junquera and P. Ghosez, J. Comput. Theor. Nanosci. **5**, 2071 (2008).
[5] C. A. Mead, Phys. Rev. Lett. **6**, 545 (1961).
[6] A. M. Bratkovsky and A. P. Levanyuk, J. Comput. Theor. Nanosci. **6**, 465 (2009).
[7] M. Stengel, D. Vanderbilt, and N. A. Spaldin, Nature Mater. **8**, 392 (2009).
[8] G. Gerra, A. K. Tagantsev, and N. Setter, Phys. Rev. Lett. **98**, 207601 (2007).
[9] J. Junquera and P. Ghosez, Nature (London) **422**, 506 (2003).
[10] C.-G. Duan, R. F. Sabirianov, W.-N. Mei, S. S. Jaswal, and E. Y. Tsymbal, Nano Lett. **6**, 483 (2006).
[11] M. Nuñez and M. Buongiorno Nardelli, Phys. Rev. Lett. **101**, 107603 (2008).
[12] X. Wu, M. Stengel, K. M. Rabe, and D. Vanderbilt, Phys. Rev. Lett. **101**, 087601 (2008).
[13] M. Stengel, N. A. Spaldin, and D. Vanderbilt, Nat. Phys. **5**, 304 (2009).
[14] A. K. Tagantsev, Ferroelectrics **375**, 19 (2008).
[15] C. Sgiarovello, M. Peressi, and R. Resta, Phys. Rev. B **64**, 115202 (2001).
[16] F. Giustino and A. Pasquarello, Phys. Rev. B **71**, 144104 (2005).
[17] N. Marzari and D. Vanderbilt, Phys. Rev. B **56**, 12847 (1997).
[18] In practice, we represent the position operator in periodic boundary conditions by means of a sawtooth function with the discontinuity placed in the region where the Wannier charge is smallest in magnitude.
[19] X. Wu, O. Diéguez, K. M. Rabe, and D. Vanderbilt, Phys. Rev. Lett. **97**, 107602 (2006).
[20] M. Stengel and N. A. Spaldin, Phys. Rev. B **75**, 205121 (2007).
[21] d can be interpreted as the time integral of the total transient current that has flowed through a facet of the supercell while adiabatically polarizing the system. This means that d is inclusive of the displacement current, which stems from variations in the macroscopic $\mathcal{E}$ even in the absence of a polarizable material.
[22] X. Wu, D. Vanderbilt, and D. R. Hamann, Phys. Rev. B **72**, 035105 (2005).
[23] We specialize here to the case in which both electrode materials are the same. Otherwise, a term should be included to reflect the different separation between the Fermi level and average electrostatic potential in the two metals.
[24] A. Baldereschi, S. Baroni, and R. Resta, Phys. Rev. B **61**, 734 (1988).
[25] P. E. Blöchl, Phys. Rev. B **50**, 17953 (1994).
[26] S. Froyen and M. L. Cohen, J. Phys. C **19**, 2623 (1986).
[27] H. J. Monkhorst and J. D. Pack, Phys. Rev. B **13**, 5188 (1976).
[28] We note that coherent $Pt/BaTiO_3/Pt$ capacitors with the in-plane lattice parameter epitaxially fixed to a thick $SrTiO_3$ substrate might be difficult to realize experimentally. Our choice of parameters was made in order to be consistent with recent first-principles studies.
[29] M. Núñez and M. Buongiorno Nardelli, Appl. Phys. Lett. **92**, 252903 (2008).
[30] I. Ponomareva, I. I. Naumov, I. Kornev, H. Fu, and L. Bellaiche, Phys. Rev. B **72**, 140102(R) (2005).
[31] C. Ederer and N. A. Spaldin, Phys. Rev. Lett. **95**, 257601 (2005).
[32] D. J. Kim, J. Y. Jo, Y. S. Kim, Y. J. Chang, J. S. Lee, J.-G. Yoon, T. K. Song, and T. W. Noh, Phys. Rev. Lett. **95**, 237602 (2005).
[33] A. Bilić and J. D. Gale, Phys. Rev. B **79**, 174107 (2009).
[34] We note that our calculated critical strain for ferroelectricity, −2.5%, is somewhat lower than the value of −5.5% predicted in Ref. 52.
[35] M. Nuñez and M. Buongiorno Nardelli, Phys. Rev. B **73**, 235422 (2006).
[36] M. Mrovec, J.-M. Albina, B. Meyer, and C. Elsasser, Phys. Rev. B **79**, 245121 (2009).
[37] M. Stengel and N. A. Spaldin, Nature (London) **443**, 679 (2006).
[38] Since we assumed $N=8$ for the nonstoichiometric symmetric geometries, each interface term contains half of the interface oxide

monolayer and one must take this into account by setting $N=7.5$ in the asymmetric case.
[39] C. Fall, N. Binggeli, and A. Baldereschi, J. Phys.: Condens. Matter **11**, 2689 (1999).
[40] I. Souza, N. Marzari, and D. Vanderbilt, Phys. Rev. B **65**, 035109 (2001).
[41] G. Gerra, A. K. Tagantsev, N. Setter, and K. Parlinski, Phys. Rev. Lett. **96**, 107603 (2006).
[42] A. K. Tagantsev, G. Gerra, and N. Setter, Phys. Rev. B **77**, 174111 (2008).
[43] W. Zhong, D. Vanderbilt, and K. M. Rabe, Phys. Rev. Lett. **73**, 1861 (1994).
[44] W. Zhong, D. Vanderbilt, and K. M. Rabe, Phys. Rev. B **52**, 6301 (1995).
[45] T. Nishimatsu, U. V. Waghmare, Y. Kawazoe, and D. Vanderbilt, Phys. Rev. B **78**, 104104 (2008).
[46] P. Ghosez and K. M. Rabe, Appl. Phys. Lett. **76**, 2767 (2000).
[47] I. I. Naumov, L. Bellaiche, and H. Fu, Nature (London) **432**, 737 (2004).
[48] S. Bin-Omran, I. Ponomareva, and L. Bellaiche, Phys. Rev. B **77**, 144105 (2008).
[49] I. Ponomareva, L. Bellaiche, and R. Resta, Phys. Rev. Lett. **99**, 227601 (2007).
[50] We expect the out-of-plane component of the local dielectric tensor, $\epsilon_{33}(x)$, to be *positive* in the middle of a PZT film which is polarized in-plane along (001) as the tetragonal state of the bulk crystal should be locally stable against rotations of P.
[51] P. Aguado-Puente and J. Junquera, Phys. Rev. Lett. **100**, 177601 (2008).
[52] O. Diéguez, K. M. Rabe, and D. Vanderbilt, Phys. Rev. B **72**, 144101 (2005).